Mean-field diffusion-limited aggregation: A "density" model for viscous fingering phenomena

Vladislav A. Bogoyavlenskiy*
Low Temperature Physics Department, Moscow State University, 119899 Moscow, Russia
(Received 25 January 2001; published 19 November 2001)

We explore a universal ''density'' formalism to describe nonequilibrium growth processes, specifically, the immiscible viscous fingering in Hele-Shaw cells (usually referred to as the Saffman-Taylor problem). For that we develop an alternative approach to the viscous fingering phenomena, whose basic concepts have been recently published in a Rapid Communication [Phys. Rev. E **63**, 045305(R) (2001)]. This approach uses the diffusion-limited aggregation (DLA) paradigm as a core: we introduce a mean-field DLA generalization in stochastic and deterministic formulations. The stochastic model, a quasicontinuum DLA, simulates Monte Carlo patterns, which demonstrate a striking resemblance to natural Hele-Shaw fingers and, for steady-state growth regimes, follow precisely the Saffman-Taylor analytical solutions in channel and sector configurations. The relevant deterministic theory, a complete set of differential equations for a time development of density fields, is derived from that stochastic model. As a principal conclusion, we prove an asymptotic equivalency of both the stochastic and deterministic mean-field DLA formulations to the classic Saffman-Taylor hydrodynamics in terms of an interface evolution.

DOI: 10.1103/PhysRevE.64.066303 PACS number(s): 47.20.Hw, 47.54.+r, 61.43.Hv, 68.03.−g

I. INTRODUCTION

Among a wide variety of natural nonequilibrium growth processes [1–9], the viscous fingering in Hele-Shaw cells has attracted much attention ever since its first experimental observation about a century ago: the forcing of a liquid into a more viscous one to recede results in the complex evolution of a moving interface between the liquids, producing a range of branched shapes [10]. In the original Hele-Shaw geometry, that phenomena are studied in a two-dimensional cell limited by closely spaced parallel solid plates; interfacial structures observed there range from smooth steady-state ''fingers'' to fractal unstable ''trees,'' depending upon such measurable quantities as the cell thickness, the surface tension, the average rate of flow, and the shear viscosity of the most viscous liquid [11–14].

Since Saffman and Taylor treated the simplest possible problem of an immiscible viscous displacement inside an infinitely long linear channel in the absence of surface tension [15], much refinement has been done in the theoretical consideration of the viscous fingering phenomena. Related investigations have been mainly devoted to generalizing the shape, stability analysis, and selection mechanisms for smooth steady-state fingers penetrating in Hele-Shaw cells of channel [16–30], sector [31–36], and radial [37–40] configurations. Nevertheless, there is still no universal formalism, which can describe as well unstable experimental regimes when producing interfacial structures demonstrate a fractal behavior [41–60]. In other words, the stochastic nature of the viscous fingering (as its essential internal property) is not underpinned yet, making an alternative approach to that phenomena to be of fundamental importance. So, this challenges us for the present work.

*Present address: Physics Department, State University of New York at Binghamton, Binghamton, NY 13902-6016. Email address: vbogoyav@binghamton.edu

The paper is organized as follows. For a background, in Sec. II we discuss two different approaches—the classic Saffman-Taylor hydrodynamics and a ''density'' formalism—to modeling the viscous fingering in Hele-Shaw cells. In Sec. III, we argue that density formalism, the subject to explore, to be based on the diffusion-limited aggregation (DLA) paradigm; so a mean-field DLA generalization in stochastic and deterministic formulations is required. In Sec. IV, we construct first the stochastic generalization, a quasicontinuum DLA model, suggesting a kinetic hypothesis for its specification. Then in Sec. V, we test the model proposed by extensive statistical studies for various two-dimensional configurations: channel, sector, and radial; we compare Monte Carlo patterns with natural Hele-Shaw fingers and, for steady-state growth regimes, with the Saffman-Taylor analytical solutions known. In Sec. VI, we introduce next the deterministic mean-field theory as a complete set of differential equations derived from an asymptotics of the quasicontinuum DLA; we study general properties of these equations, including a stability analysis, and examine their two-dimensional solutions by a comparison with the Saffman-Taylor ones in the same spatial configurations as in Sec. V. After that in Sec. VII, we justify the kinetic hypothesis suggested in the beginning of our stochastic framework. Finally, Sec. VIII makes a conclusion.

II. BACKGROUND

Before we focus on the specific problem of an interface evolution between two immiscible liquids in a Hele-Shaw cell, let us raise and discuss a background question: by which terms can, in principle, the dynamics of a continuum medium be formulated? A solution is not implied definitely since at least two different approaches are valid. Following a regular way, one has to determine a velocity vector $\mathbf{v}(\mathbf{r},t)$ and its time development in each point of the medium. Alternatively, one has to determine a medium density $\rho(\mathbf{r},t)$ as a function of time and spatial coordinates. In this connection, the vis-

cous fingering may be considered from the two points of view: (i) as a hydrodynamic problem (the velocity formalism) or (ii) as a nonequilibrium growth process (the density formalism); we will describe both in detail below.

A. Velocity formalism

The classic hydrodynamic theory for the immiscible viscous displacement in Hele-Shaw cells was introduced by Saffman and Taylor in 1958 [15]. By this approach, a two-dimensional field of the liquid velocity $\mathbf{v}(\mathbf{r},t)$ is studied in terms of a potential function ψ,

$$\mathbf{v}(\mathbf{r},t)=\boldsymbol{\nabla}\psi(\mathbf{r},t). \tag{1}$$

Then the Saffman-Taylor problem involves solving a bulk incompressibility equation

$$\nabla^2\psi(\mathbf{r},t)=0 \tag{2}$$

coupled with boundary conditions

$$\psi|_{\mathbf{r}\in\Gamma(t)}=d_0\kappa|_{\mathbf{r}\in\Gamma(t)}, \tag{3}$$

$$(\boldsymbol{\nabla}\psi)_{\mathbf{n}}=\left(\frac{\partial\Gamma}{\partial t}\right)_{\mathbf{n}}, \tag{4}$$

where $\Gamma(t)$ denotes a moving liquid-liquid interface (with the curvature κ) which evolution we want to track, $\mathbf{n}$ indicates a direction normal to the interface, and d_0 is a dimensionless surface-tension coefficient. Here, Eq. (3) sets the velocity potential ψ on the curved front $\Gamma(t)$, and Eq. (4) accounts for a continuity relation.

This Saffman-Taylor formulation, Eqs. (1)–(4), specifies the interface dynamics $\Gamma(t)$ completely: the Laplace bulk law [Eq. (2)] with the Dirichlet boundary condition [Eq. (3)] determine the flow potential $\psi(\mathbf{r},t)$, and after that its normal component at the front gives the interface velocity $\partial\Gamma/\partial t$ [Eq. (4)]. Thus, we have a Stefan, or moving-boundary-value problem.

B. Density formalism

In contrast to the well-studied hydrodynamic description of the immiscible viscous fingering (referred to as the Saffman-Taylor problem), the density formalism for that phenomena has not been explored enough. Nevertheless, its foundation stone appears to be rather clear and is formulated as follows. Let a continuous function

$$\rho(\mathbf{r},t)\in[0,\ldots,\rho^*] \tag{5}$$

define the density of a ''finger'' (an equivalent of the less viscous liquid) which grows in a ''nutrient'' (an equivalent of the most viscous liquid) field $u(\mathbf{r},t)$. We consider a mean density $\rho^*/2$ to determine the finger region $\Phi(t)$ and the finger front $\Gamma(t)$ (an equivalent of the liquid-liquid interface) as

$$\rho|_{\mathbf{r}\in\Phi(t)}>\frac{\rho^*}{2},\quad \rho|_{\mathbf{r}\in\Gamma(t)}=\frac{\rho^*}{2}. \tag{6}$$

To propose a model, one has to introduce a complete set of differential equations for a time development of the functions $\rho(\mathbf{r},t)$ and $u(\mathbf{r},t)$.

While the nutrient density $u(\mathbf{r},t)$, a passive growth field, obeys the Laplace law $\nabla^2u=0$ at $\partial\rho/\partial t=0$, a mass conservation in the finger/nutrient system is implied as

$$\frac{\partial\rho(\mathbf{r},t)}{\partial t}=\nabla^2u(\mathbf{r},t). \tag{7}$$

For the formulation to be specified completely, we need to couple Eq. (7) with a kinetic relation for the finger growth rate,

$$\frac{\partial\rho(\mathbf{r},t)}{\partial t}=\hat{F}\{u(\mathbf{r},t),\rho(\mathbf{r},t)\}, \tag{8}$$

where $\hat{F}$ denotes a functional operator of $\rho(\mathbf{r},t)$ and $u(\mathbf{r},t)$, the key aspect of the formalism. A general form of that operator is determined from the Boltzmann kinetic theory [61]:

$$\hat{F}(\mathbf{r},t)=\int_{\mathbf{r}+\mathbf{e}\in I(t)}u(\mathbf{r},t)\rho(\mathbf{r}+\mathbf{e},t)w(\mathbf{r},\mathbf{e},t)dI. \tag{9}$$

Here, we consider a nonequilibrium process of the finger growth as a two-particle interaction between the finger $[\rho(\mathbf{r}+\mathbf{e},t)]$ and nutrient $[u(\mathbf{r},t)]$ fields; the integration is performed inside a collision sphere $\mathbf{r}+\mathbf{e}\in I(t)$, the interaction spatial region; the factor $w(\mathbf{r},\mathbf{e},t)$ sets there the distribution function of a successful collision, the interaction intensity.

This density formulation, Eqs. (5)–(9), however, contains the serious gap, *a priori* unknown operator $\hat{F}$; indeed, we can neither predetermine nor guess the kinetic parameters $I(t)$ and $w(\mathbf{r},\mathbf{e},t)$ in Eq. (9). We know only an output of the problem: the finger density field $\rho(\mathbf{r},t)$ should reproduce the Saffman-Taylor hydrodynamics [Eqs. (1)–(4)] in terms of the interface evolution $\Gamma(t)$. Thus, what can we do in such deadlock? In order to solve the puzzle of unknown kinetics, we plan a reversible metamorphosis in the two steps: (i) first, we reduce the continuum deterministic formulation given above to a discrete stochastic one for which the parameters $I(t)$ and $w(\mathbf{r},\mathbf{e},t)$ would be specified statistically and then verified and justified by Monte Carlo simulations; (ii) after that, a backward discrete-continuum transition will yield the operator $\hat{F}$ *a posteriori*.

III. DIFFUSION-LIMITED AGGREGATION

The basic discrete model adapted for stochastic simulations of nonequilibrium growth processes in Laplacian systems, the diffusion-limited aggregation (DLA), was originally introduced by Witten and Sander in 1981 [62]. Its rules are very simple: a cluster of particles expands via successive attachment of growth units being sent, one at a time, from a far source and then randomly walking on a lattice; the attachment occurs when a growth unit reaches a neighboring site of the pre-existing cluster [63]. Remarkably, Monte Carlo algorithms of that kind are well-known to simulate fractal

ramified patterns that resemble the unstable viscous finger morphologies observed in natural porous media [64–73].

As was first noted by Paterson [74] and then universally recognized, growth equations for the DLA model are similar to the Saffman-Taylor ones in case of an infinitesimal surface tension. In fact, the role of the velocity potential ψ is played for DLA by the probability P_v of visiting a lattice site; that probability similarly obeys the Laplace law $\nabla^2 P_v = 0$ [Eq. (2)] whereas the normal growth velocity at a cluster front is directly proportional to the P_v gradient [Eq. (4)]. Thus, one may conclude the DLA paradigm to reproduce the Saffman-Taylor hydrodynamic solutions in a mean-field limit [11,74–84], in agreement with a resemblance between contour plots of ensemble-averaged DLA clusters and natural shapes of steady-state fingers penetrating in Hele-Shaw cells [85,86].

Although fundamental capability of DLA-based algorithms to simulate the viscous fingering phenomena appears to be obvious, the adequate formulation of a mean-field DLA theory, i.e., a valid transition from discrete growth units to continuum density fields, has been a challenge for the last two decades. The main problem stems from the existence of a surface tension in the hydrodynamics, the coefficient d_0 in Eq. (3), which has no counterpart in the Witten-Sander DLA [62]. Indeed, the surface tension implies a capillary length l_c, the characteristic scale of a steady-state behavior for the Saffman-Taylor solutions [17–21]; for regular DLA patterns, however, this scale equals a lattice spacing so it seems quite impossible to consider a ''stable zone'' on a fractal cluster.

There has been a number of attempts to introduce the capillary length l_c to the DLA model in a heuristic way. Modifications of growth rules and conditions proposed for that include principally the following: (i) variation of an aggregation probability in order to the number of nearest cluster ''neighbors'' or, more generally, as a function of front curvature [87–91], (ii) application of multiple-hit averaging schemes, which vanish a statistical noise [75,92–97], and (iii) taking into account a surface diffusion of growth units and the thermodynamics related [98–100]. Unfortunately, none of these DLA modifications operates with finite spatial distributions of a cluster density field $\rho(\mathbf{r},t)$, which is essential for subsequent derivation of a continuum theory.

Among miscellaneous continuum approaches introduced for the DLA model so far [62,101–111], the vast majority suffers from a lack of *ab initio* principles. The reason is discussed in the previous section: to construct a mean-field theory, one has to suggest a hypothesis on the aggregation kinetics [Eq. (9)], which cannot be explicitly verified and justified for a purely continuum, deterministic formulation. But this difficulty surprisingly disappears as we construct the mean-field DLA theory on the basis of a quasicontinuum (still stochastic) framework, the subject of Sec. IV. Then we can apply statistical methods to verify and justify that aggregation kinetics (Sec. V), and can next proceed from the quasicontinuum DLA to the relevant deterministic mean-field theory (Sec. VI). As an advantage, such plan allows us to establish valid connections to both stochastic and deterministic DLA originals for all steps of the derivation.

IV. QUASICONTINUUM DLA MODEL

A quasicontinuum generalization of the regular on-lattice DLA algorithm is introduced as follows [112]. Let us consider an integer positive number K, the discreteness parameter of the cluster density field $\rho(\mathbf{r},t)$; for a lattice site, the value of ρ is an element of the finite set,

$$\rho(\mathbf{r},t) \in \left[0, \frac{1}{K}, \frac{2}{K}, \ldots, \frac{K-2}{K}, \frac{K-1}{K}, 1\right], \tag{10}$$

i.e., a stairlike distribution is substituted for the continuous function $\rho(\mathbf{r},t)$ in Eq. (5). A mass diffusion is simulated by the flux of ''walkers'' (growth units) transferring a constant portion $u_0 \equiv 1/K$ from a far source to the expanding cluster field. Since this quasicontinuum framework provides nonempty spectrum of ρ values between the extremes 0 and 1, a subdivision of whole $\mathbf{r}$ space into ''unoccupied'' ($\rho=0$) and ''occupied'' ($\rho=1$) lattice sites (as in the Witten-Sander algorithm) is no more appropriate. The formerly sharp cluster front (a jump from 0 to 1) becomes an intermediate region over which the density field $\rho(\mathbf{r},t)$ varies (by discrete portions $1/K$) between zero and a stationary eigenvalue ρ^*. So the quasicontinuum DLA model implies a probability of walker aggregation $P(\mathbf{r},t)$ to be dependent not on the presence (or absence) of nearest occupied sites, but rather on the average cluster density in a neighborhood of that walker.

In order to define the aggregation probability $P(\mathbf{r},t)$, we transform a continuum expression for the Boltzmann collision integral [Eq. (9)] to its lattice analog,

$$P(\mathbf{r},t) = \sum_i \rho(\mathbf{r}+\mathbf{e}_i,t) w(\mathbf{r},\mathbf{e}_i,t), \tag{11}$$

where the collision sphere $I(t)$ is considered to include the sites $\mathbf{r}+\mathbf{e}_i$ adjacent to $\mathbf{r}$, and the index i runs over different neighbors. Here, we have already specified one kinetic parameter by Eq. (11), the interaction region $I(t)$; but the other, the interaction intensity $w(\mathbf{r},\mathbf{e}_i,t)$, remains undefined yet. To suggest a hypothesis on its form, we satisfy the following three premises:

(i) All the neighboring sites $\mathbf{r}+\mathbf{e}_i$ are equivalent for the aggregation process, i.e., the interaction intensity $w(\mathbf{r},\mathbf{e}_i,t) \equiv w(\mathbf{r},t)$ does not depend on the index i.

(ii) Due to the linear stability of a cluster front against infinitesimal perturbations, there is imposed a threshold growth condition at small neighboring densities,

$$w(\mathbf{r},t) \to 0 \text{ as } \rho(\mathbf{r}+\mathbf{e}_i,t) \to 0. \tag{12}$$

(iii) The function $w(\mathbf{r},t)$ is an isometric invariant and, therefore, it should yield isotropic density measure.

Upon the requirements (i)–(iii) listed above, we introduce the interaction intensity as

$$w(\mathbf{r},t) = \sum_i \rho(\mathbf{r}+\mathbf{e}_i,t). \tag{13}$$

This relation concludes our definition of the aggregation probability $P(\mathbf{r},t)$; combining Eqs. (11) and (13), one obtains

$$P(\mathbf{r},t)=\left\langle \sum_i \rho(\mathbf{r}+\mathbf{e}_i,t) \right\rangle^2. \tag{14}$$

Thus, the quasicontinuum DLA formulation is specified: while a walker released from the source executes stochastic motion, at each time step a real random number $R \in (0,\ldots,1)$ is generated and compared with the aggregation probability $P(\mathbf{r},t)$ being determined from Eq. (14). If the inequality $R<P(\mathbf{r},t)$ is valid, the walker aggregates into the lattice site and advances the cluster density at that point, $\rho(\mathbf{r},t)$, by the value of u_0; otherwise, $R \geqslant P(\mathbf{r},t)$, stochastic wandering is continued until the walker aggregates elsewhere on the cluster. As successive walkers repeat such procedure, the density field $\rho(\mathbf{r},t)$ is modified in time. For $K=1$, this Monte Carlo algorithm coincides with the regular Witten-Sander one [62]; the model converges to a mean-field DLA limit when the discreteness parameter goes to infinity, $K\to\infty$.

V. STATISTICAL STUDIES

In order to test the quasicontinuum DLA model introduced in the previous section, we take a square grid $\mathbf{r}=(x,y)$ of spacing a and consider there only nearest-neighborhood interactions; so the corresponding on-square-lattice aggregation probability $P(x,y,t)$ is determined from the formula

$$P(x,y,t)=\langle \rho(x+a,y,t)+\rho(x-a,y,t)+\rho(x,y+a,t) + \rho(x,y-a,t)\rangle^2. \tag{15}$$

In this section, we will apply our model for various two-dimensional configurations: channel, sector, and radial.

A. Channel configuration

Let us start statistical studies from the classic Saffman-Taylor configuration, an infinitely long linear channel of width W [15]. A translation invariance of this problem implies the normal reflection condition for wandering walkers on lateral walls, $y=\pm W/2$; we locate a growth nucleus at the origin $(0,0)$.

In Fig. 1, we present Monte Carlo results for a channel of width $W=64a$ where the discreteness parameter K is varied in the range $[1,\ldots,2^{12}]$. For $K=1$, a regular DLA cluster is simulated [Fig. 1(a)]; increase of K leads to a successive thickening of cluster branches [Fig. 1(b)], and the last two patterns [Figs. 1(c) and 1(d)] look like unstable viscous fingers observed experimentally in rectilinear Hele-Shaw cells [41–49]. Thus, our quasicontinuum generalization of DLA yields the capillary length scale l_c as a monotonic function of K, which raises the next problem: how to vary this scale principally, to enlarge it up to values comparable with the channel width W, to reproduce steady-state Saffman-Taylor fingers?

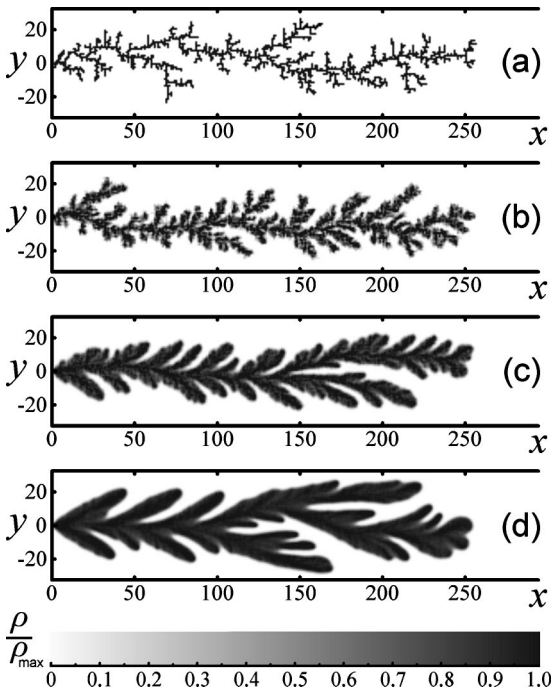

FIG. 1. Quasicontinuum DLA simulation on a square grid (x,y) of spacing $a=1$ inside a channel of width $W=64a$. Aggregation probability $P(x,y,t)$ is set by Eq. (15); discreteness $K=1$, 2^4, 2^8, and 2^{12} for plots (a), (b), (c), and (d), respectively.

The simplest solution to enlarge l_c consists in the further increase of the parameter K. To elaborate such way, we have calculated a mean capillary length, the average over an ensemble of similar clusters; results are plotted in Fig. 2. Unfortunately, we conjecture the functional dependence $l_c(K)$ to be too weak,

$$l_c(K)\propto \log K, \tag{16}$$

so this way is unpromising since, e.g., steady-state fingers inside the channel of width $W=64a$ cannot be simulated even as $K=2^{20}$.

In order to derive a more efficient mechanism to enlarge l_c without substantial increase of computational time (which is directly proportional to K), let us discuss an origin

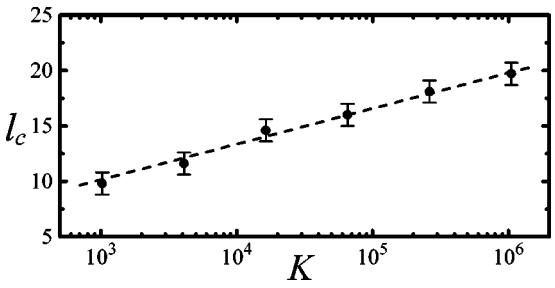

FIG. 2. Capillary length l_c as a function of discreteness parameter K (see Fig. 1). Monte Carlo data (solid circles with error bars) are interpolated by a dependence $l_c(K)\propto \log K$ (dash line) conjectured.

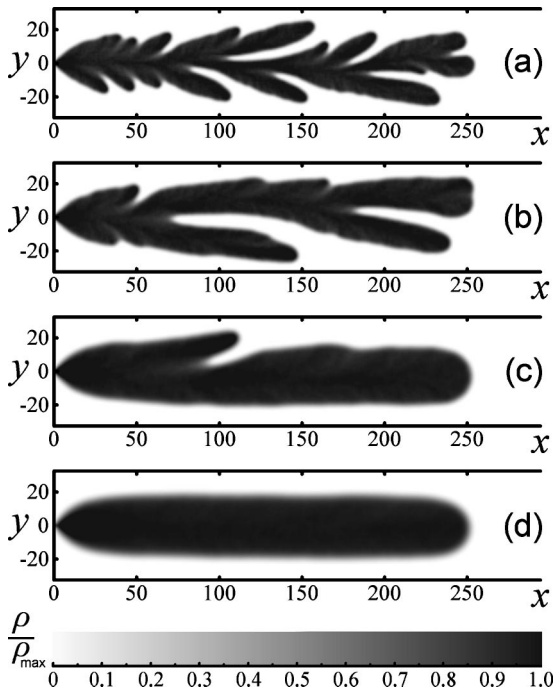

FIG. 3. ξ-modified quasicontinuum DLA simulation on a square grid (x,y) of spacing $a=1$ inside a channel of width $W=64a$. Aggregation probability $P(x,y,t)$ is set by Eq. (18) with $\xi=1$, 2, 3, and 3(1/2) for plots (a), (b), (c), and (d), respectively; discreteness is fixed, $K=2^{12}$.

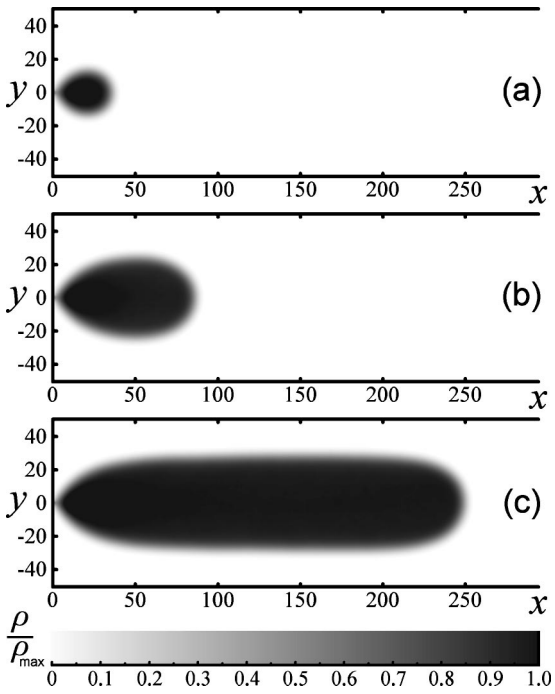

FIG. 4. ξ-modified quasicontinuum DLA simulation on a square grid (x,y) of spacing $a=1$ inside a channel of width $W=100a$. Aggregation probability $P(x,y,t)$ is set by Eq. (18) with $\xi=3(3/4)$ ($\delta=2a$); discreteness $K=2^{12}$. We present different stages of a steady-state front propagation: (a) nucleation, (b) tip formation, and (c) stationary growth.

of the length scale in the model. In fact, the sum of neighboring cluster densities in Eq. (15) represents a lattice Laplacian,

$$P(x,y,t)\propto\left[1+\frac{a^2}{4}\nabla^2\right]\rho(x,y,t). \tag{17}$$

By this relation, the capillary length l_c originates from a term $(a^2/4)^{1/2}=a/2$, the characteristic small scale of the square grid of spacing a. Hence, the replacement $a^2/4\leftrightarrow\delta^2$ in Eq. (17) changes that microscale from $a/2$ to δ, which modifies the aggregation probability formula from Eq. (15) to

$$P(x,y,t)=\langle\rho(x+a,y,t)+\rho(x-a,y,t)+\rho(x,y+a,t)+\rho(x,y-a,t)-\xi\rho(x,y,t)\rangle^2, \tag{18}$$

where the factor ξ and the microscale δ are connected as

$$\xi=4-\frac{a^2}{\delta^2}\Leftrightarrow\delta=\frac{a}{\sqrt{4-\xi}}. \tag{19}$$

As illustrated in Fig. 3, the variation of ξ in the range $[0,\ldots,4)$ allows us to govern the capillary length $l_c\propto\delta$ very efficiently. Inside the same channel of width $W=64a$, Monte Carlo runs for $\xi=1$, 2, and 3 [Figs. 3(a), 3(b), and 3(c), respectively] simulate still unstable viscous fingers with remarkable effects of tip splitting, side branching, and wobbling, related to natural Hele-Shaw structures [41–49]. When we put $\xi=3(1/2)$ [Fig. 3(d)], the capillary length l_c increases enough to provide a steady-state front propagation so the density field $\rho(x,y,t)$ reproduces a single Saffman-Taylor finger [42,46].[1]

For a detailed analysis of that steady-state regime, we consider a wider channel, $W=100a$, and apply the ξ-modified quasicontinuum DLA model [Eq. (18)] with $\delta=2a$; results are shown in Fig. 4. Here, the growth dynamics is subdivided conditionally into three stages as follows. First, there is a dropletlike nucleation [Fig. 4(a)] as the finger settles at the origin. When the finger width becomes comparable with $W/2$ [Fig. 4(b)], lateral walls begin to form a tip shape. In a final stage, the stationary growth [Fig. 4(c)], the steady-state front propagates through the channel with a constant velocity whereas the tip shape of the finger is an invariant.

Data treatments for Fig. 4 are summarized in Fig. 5; there we compute longitudinal [Fig. 5(a)] and transverse [Fig. 5(b)] profiles of the density field $\rho(x,y,t)$ for the three growth stages mentioned above. For the stationary stage

[1]As a consequence, the quasicontinuum DLA gives us an algorithm for an ensemble averaging of regular DLA clusters, opposite to the multiple-hit one proposed by Tang in 1985 [75]. Making a principal difference from Tang's purely discrete scheme, the quasicontinuum DLA operates with finite spatial distributions of the density field $\rho(\mathbf{r},t)$, whereas computational rates of these two averaging schemes are approximately equal.

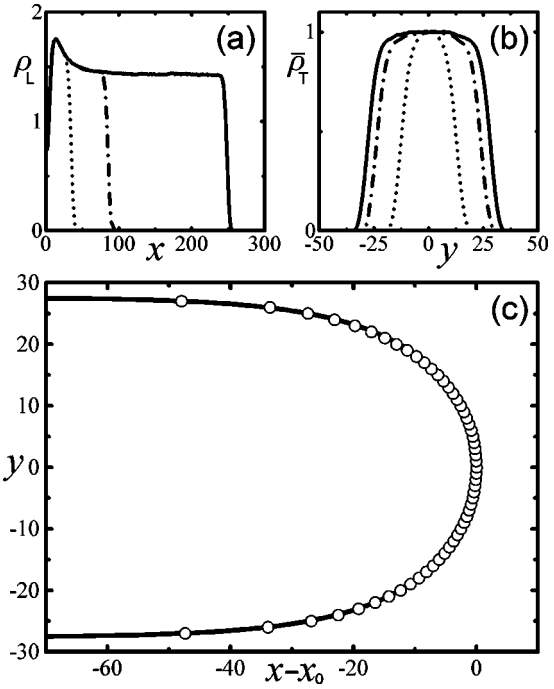

FIG. 5. Data treatments for Fig. 4. (a) Longitudinal profiles, $\rho_L(x,t)\equiv\rho(x,y=0,t)$, for Fig. 4(a) (dot curve), Fig. 4(b) (dot-dash curve), and Fig. 4(c) (continuous curve). (b) Normalized transverse profiles, $\overline{\rho_T}(y,t)\equiv\rho(x^*,y,t)/\rho(x^*,y=0,t)$, in sections of a maximal finger width, $x=x^*$, for Fig. 4(a) (dot curve), Fig. 4(b) (dot-dash curve), and Fig. 4(c) (continuous curve). (c) Contour plot of a mean density at finger tip (open circles) for a stationary growth stage [see Fig. 4(c)], compared with the Saffman-Taylor analytical solution by Eq. (21) (continuous curve) as $\lambda=0.554$.

[Fig. 4(c)], the relevant transverse profile $\overline{\rho_T}$ [continuous curve in Fig. 5(b)] approaches a step function as is required;[2] a relative finger width λ measured at the midheight of that stationary distribution gives the value $\lambda=0.554$, the result of the Saffman-Taylor problem extended for a finite surface tension [22–24],

$$\lambda(l_c)=\frac{1}{2}+0.114\left(\frac{l_c}{W}\right)^{4/3}, \tag{20}$$

with $l_c\approx 57a$. At the finger tip, the contour plot of a mean density [Fig. 5(c)] follows precisely the Saffman-Taylor analytical solution [15]

$$x(y)-x_0=\frac{W(1-\lambda)}{2\pi}\ln\left[\frac{1}{2}\left(1+\cos\frac{2\pi y}{\lambda W}\right)\right], \tag{21}$$

where x_0 is the tip position as $y=0$.

[2]A liquid flow being modeled by the finger density field $\rho(\mathbf{r},t)$ predetermines naturally the step-type conditions: $\rho=$const within the finger region $\Phi(t)$ (the less viscous liquid) and $\rho=0$ elsewhere (the most viscous liquid); this will be also discussed in Sec. VI.

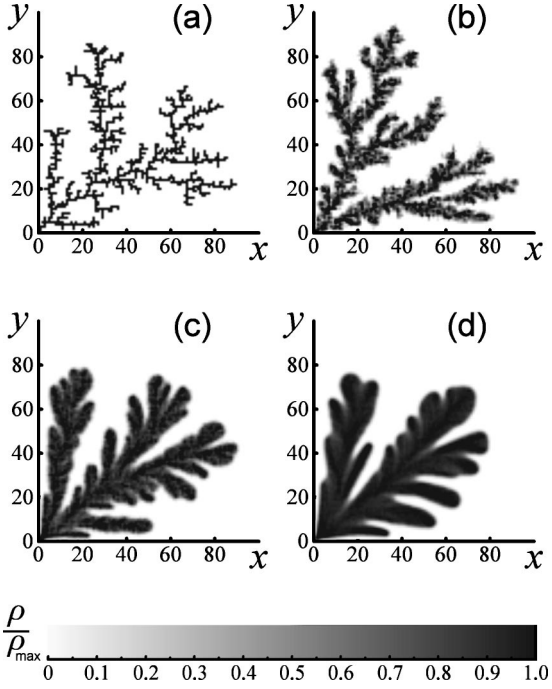

FIG. 6. Quasicontinuum DLA simulation on a square grid (x,y) of spacing $a=1$ inside a sector of right angle, $\theta_0=90°$ ($x>0$ and $y>0$). Aggregation probability $P(x,y,t)$ is set by Eq. (15); discreteness $K=1$, 2^4, 2^8, and 2^{12} for plots (a), (b), (c), and (d), respectively.

B. Sector configuration

Encouraged by a success of the quasicontinuum DLA in modeling the viscous fingering in channels, we switch to the next important two-dimensional configuration, a sector-shaped Hele-Shaw cell of angle θ_0 [50]. For this problem, we will use polar spatial coordinates, the radius r, and the angle $\theta\in[-\theta_0/2,\ldots,\theta_0/2]$, as well as the Cartesian basis (x,y) for which the conversion formulas needed are

$$x=r\cos\left(\theta+\frac{\theta_0}{2}\right),\quad y=r\sin\left(\theta+\frac{\theta_0}{2}\right). \tag{22}$$

In statistical studies, we impose the normal reflection condition for wandering walkers on sector walls, $\theta=\pm\theta_0/2$, and locate a growth nucleus at the origin $(0,0)$.

1. Sector $\theta_0=90°$

Let us consider first a sector of right angle, $\theta_0=90°$, assigned to the main quarter of the square (x,y) grid ($x>0$ and $y>0$). In Figs. 6 and 7, we present Monte Carlo results for this 90° sector where the aggregation probability $P(x,y,t)$ is set by Eqs. (15) and (18), respectively. Similar to the channel configuration investigated before, our model allows us to reproduce all basic properties of natural Hele-Shaw structures [49,50], i.e., (i) a steady-state front propagation within the capillary length scale l_c [which increases with K and ξ, following Eqs. (16) and (19)], and (ii) a fractal growth on larger scales.

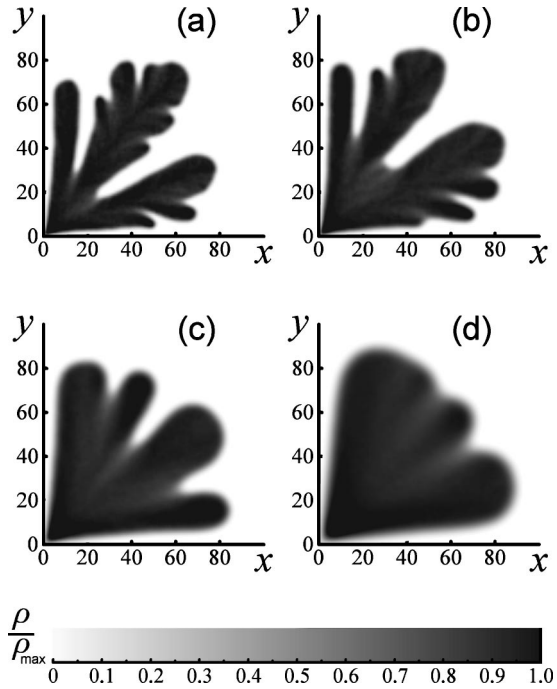

FIG. 7. ξ-modified quasicontinuum DLA simulation on a square grid (x,y) of spacing $a=1$ inside a sector of right angle, $\theta_0=90°$ ($x>0$ and $y>0$). Aggregation probability $P(x,y,t)$ is set by Eq. (18) with $\xi=1$, 2, 3, and 3(1/2) for plots (a), (b), (c), and (d), respectively; discreteness is fixed, $K=2^{12}$.

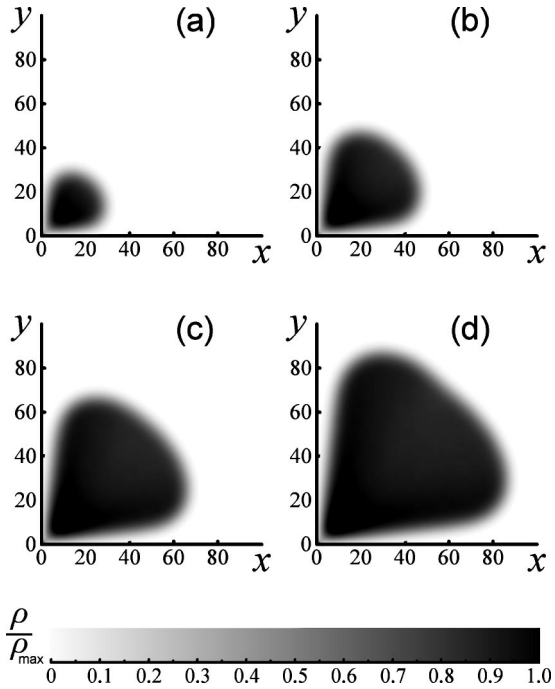

FIG. 8. ξ-modified quasicontinuum DLA simulation on a square grid (x,y) of spacing $a=1$ inside a sector of right angle, $\theta_0=90°$ ($x>0$ and $y>0$). Aggregation probability $P(x,y,t)$ is set by Eq. (18) with $\xi=3(3/4)$ ($\delta=2a$); discreteness $K=2^{12}$. We present successive pictures of a steady-state front propagation as a finger gyration radius increases: $r_g=40a$, $60a$, $80a$, and $100a$ for plots (a), (b), (c), and (d), respectively.

To analyze that steady-state regime in detail, we apply the ξ-modified quasicontinuum DLA model [Eq. (18)] with $\delta=2a$. In Fig. 8, we show the sector growth dynamics as a finger gyration radius r_g increases; the last plot, Fig. 8(d), illustrates an edge of the capillary scale when a tip shape is perturbed partially. Resembling a natural behavior [50], the statistical finger tends to occupy a well-resolved sector fraction λ_θ, an invariant in the steady-state regime. Besides, the value $\lambda_\theta=0.81$ measured at the midheight of a quasistationary azimuthal profile $\overline{\rho_A}$ is in agreement with estimations $\lambda_\theta(90°)=(0.805\pm0.02)$ from a relation

$$\lambda_\theta(\theta_0)=\frac{1}{2}+(0.0034\pm0.0002)\,\theta_0 \tag{23}$$

adapted for experimental fingers in sector-shaped Hele-Shaw cells [50,85].

Data treatments for Fig. 8 are summarized in Fig. 9; there we compute radial [Fig. 9(a)] and azimuthal [Fig. 9(b)] profiles of the density field $\rho(r,\theta,t)$. To describe the contour plot of a mean finger density [Fig. 9(c)], we perform a conformal transformation of the linear Saffman-Taylor problem [15] to polar coordinates (r,θ); see Appendix A. As a result, the dependence derived [Eqs. (A2) and (A3), continuous curve in Fig. 9(c)] describes precisely that mean contour [open circles in Fig. 9(c)] as $\lambda_\theta=0.81$, so the classic Saffman-Taylor family of solutions [Eq. (21)] appears to have a valid extension for sectors.[3]

2. *Sectors* $\theta_0=45°$, $135°$, *and* $180°$

In order to advance our comprehension of the viscous fingering in the sector configuration, let us consider some more angles: $\theta_0=45°$, 135°, and 180°. On the square (x,y) grid, we define these sectors as ($x>y$ and $y>0$), ($x>-y$ and $y>0$), and ($y>0$), respectively.

In Fig. 10, we present steady-state fingers grown by the ξ-modified quasicontinuum DLA [Eq. (18)] with $\delta=2a$. A surprising result is that all the fingers simulated tend to occupy still fixed sector fractions $\lambda_\theta<1$ even as $\theta_0=180°$. This disproves a speculative suggestion about the existence of a ''critical'' point $\theta_0^*\approx144°$ so that the relative angular

[3]This is in contradiction with the other theory developed in Refs. [31–33] according to which the sector family of solutions differs significantly from the Saffman-Taylor conformal transformation by Eq. (A1). Nevertheless, a recent investigation of mean occupancy distributions for off-lattice DLA clusters grown in the sector configuration reports the results supporting our conclusion; see Figs. 19 and 20 of Ref. [86].

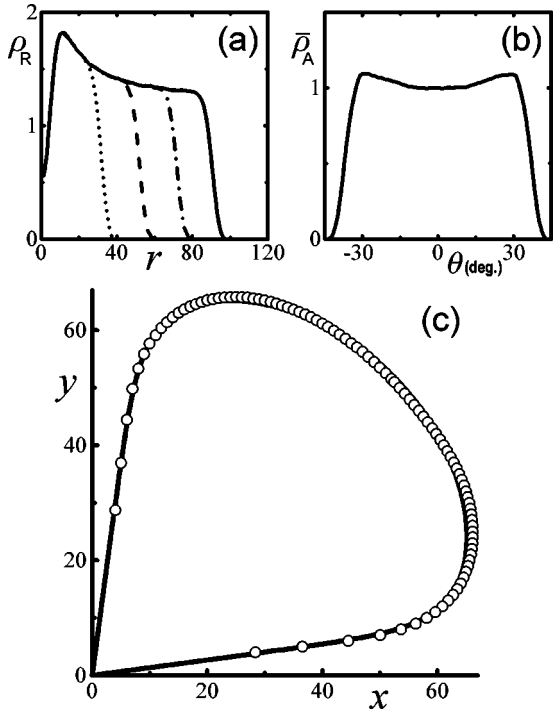

FIG. 9. Data treatments for Fig. 8. (a) Radial profiles, $\rho_R(r,t) \equiv \rho(r,\theta=0°,t)$, for Fig. 8(a) (dot curve), Fig. 8(b) (dash curve), Fig. 8(c) (dot-dash curve), and Fig. 8(d) (continuous curve). (b) Normalized azimuthal profile, $\overline{\rho_A}(\theta) \equiv \rho(r^*,\theta)/\rho(r^*,\theta=0°)$, in a quasistationary section, $r^*=50a$, for Fig. 8(c). (c) Contour plot of a mean density (open circles) for a finger of gyration radius $r_g = 80a$ [see Fig. 8(c)], compared with the Saffman-Taylor conformal transformation by Eqs. (A2) and (A3) (continuous curve) as $\lambda_\theta = 0.81$. Angle θ is measured in respect to a bisector ray ($x=y$, $x>0$) in counterclockwise direction.

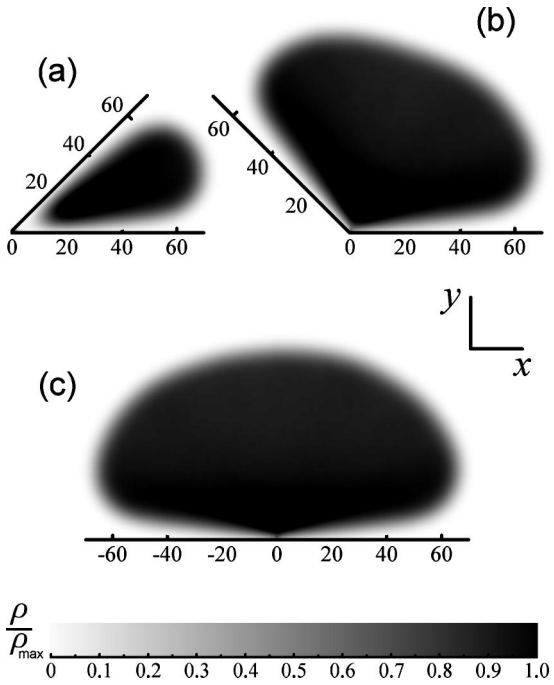

FIG. 10. ξ-modified quasicontinuum DLA simulation on a square grid (x,y) of spacing $a=1$ inside sectors $\theta_0=45°$ ($x>y$ and $y>0$), 135° ($x>-y$ and $y>0$), and 180° ($y>0$) for plots (a), (b), and (c), respectively. Aggregation probability $P(x,y,t)$ is set by Eq. (18) with $\xi=3(3/4)$ ($\delta=2a$); discreteness is fixed, $K=2^{12}$.

width $\lambda_\theta(\theta_0)$ equals 1 for $\theta_0 > \theta_0^*$ [113,114].[4] Thus, we have to revise and correct the linear connection $\lambda_\theta(\theta_0)$ by Eq. (23) which is appropriate only for small and moderate sector angles, $\theta_0 \lesssim 90°$.

As argued in Appendix B, the relative angular width λ_θ as a function of θ_0 would be approximated by the formula (θ_0 values are assumed in radians)

$$\lambda_\theta(\theta_0) = \frac{1}{2} + \frac{\theta_0}{\pi\left(4-\pi+\frac{\theta_0}{2}\right)}. \tag{24}$$

The validity of this approximation is demonstrated in Fig. 11—the function $\lambda_\theta(\theta_0)$ proposed fits very well both experimental [50] and Monte Carlo (Figs. 8 and 10) data; moreover, this describes the Hele-Shaw experiments even better than by Eq. (23) which has been originally introduced [50,85]. It is worth to mention that finger contour plots follow precisely the relevant Saffman-Taylor conformal transformations [Eq. (A1)] as λ_θ is determined from Eq. (24) for all the sectors $\theta_0 \in [45°, \ldots, 180°]$ examined.

C. Radial configuration

Finally, let us consider the quasicontinuum DLA model in a radial (sometimes referred to as circular) configuration, a limit of the previous sector problem, $\theta_0 \to 360°$. In statistical studies, we locate a growth nucleus at the origin (0,0) of the square (x,y) grid; there are no external walls for wandering walkers to reflect.

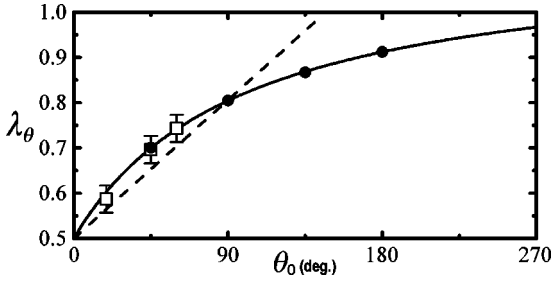

FIG. 11. Relative angular width λ_θ as a function of sector angle θ_0 (in degrees). We combine experimental data (open squares with error bars) for sectors $\theta_0=20°$, 45°, and 60° (see Ref. [50]) with Monte Carlo ones (solid circles) taken from Figs. 8 and 10 for $\theta_0 = 45°$, 90°, 135°, and 180°; we plot also a linear interpolation by Eq. (23) (dash line) and an approximation by Eq. (24) proposed (continuous curve).

[4]If one extrapolates the linear function $\lambda_\theta(\theta_0)$ by Eq. (23) for larger θ_0 values, it will be expected to reach 1 as $\theta_0^* \approx 144°$. However, any direct evidence of that suggestion is absent while the angular range for the steady-state front propagation in sectors has been reported to have an experimental limit, $\theta_0^{max} \simeq 90°$ [50].

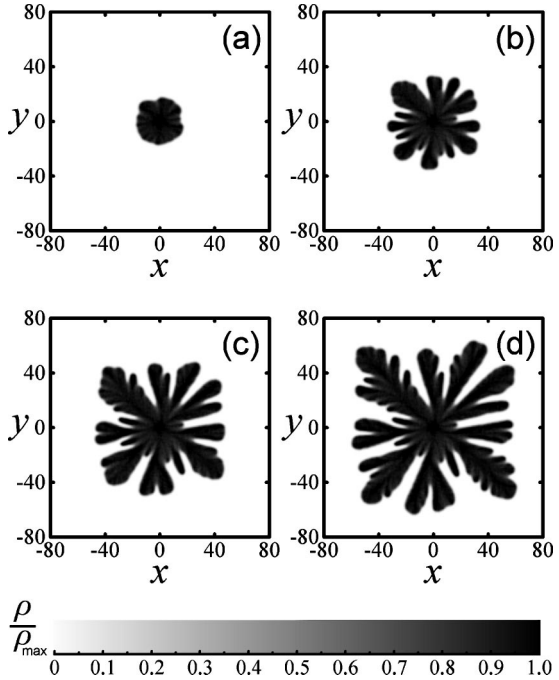

FIG. 12. Quasicontinuum DLA simulation on a square grid (x,y) of spacing $a=1$ in a radial configuration. Aggregation probability $P(x,y,t)$ is set by Eq. (15) ($\delta=a/2$); discreteness $K=2^{12}$. We present successive pictures as a gyration radius increases: $r_g=20a$, $40a$, $60a$, and $80a$ for plots (a), (b), (c), and (d), respectively.

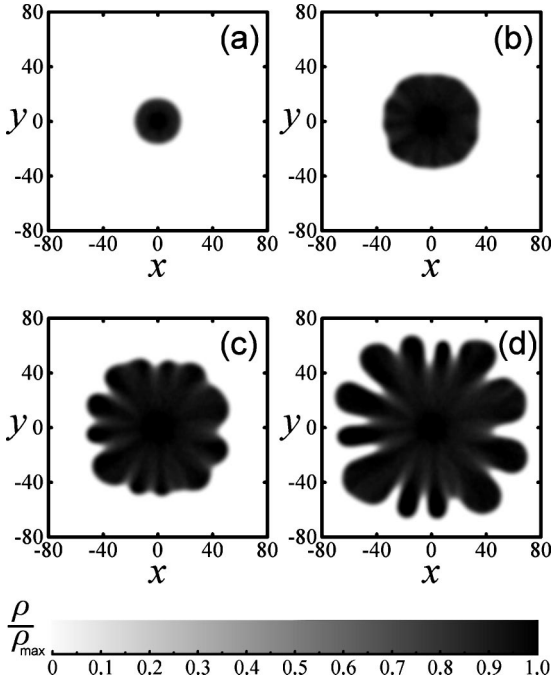

FIG. 13. ξ-modified quasicontinuum DLA simulation on a square grid (x,y) of spacing $a=1$ in a radial configuration. Aggregation probability $P(x,y,t)$ is set by Eq. (18) with $\xi=3$ ($\delta=a$); discreteness $K=2^{12}$. We present successive pictures as a gyration radius increases: $r_g=20a$, $40a$, $60a$, and $80a$ for plots (a), (b), (c), and (d), respectively.

In Figs. 12 and 13, we show the radial growth dynamics as a capillary length scale $l_c \propto \delta$ varies by the factor of two: the aggregation probability $P(x,y,t)$ is set by Eq. (15) ($\delta=a/2$) and Eq. (18) ($\delta=a$), respectively. One can resolve Monte Carlo patterns obtained to resemble the well-known behavior of natural structures in radial Hele-Shaw cells [51–60], i.e., a steady-state front propagation at small gyration radii, $r_g \lesssim l_c$ [Figs. 12(a), 13(a), and 13(b)], then a destabilization phase at an edge of the capillary scale, $r_g \simeq l_c$ [Figs. 12(b), 13(c), and 13(d)], which subsequently initiates a fractal growth as $r_g \gtrsim l_c$ [Figs. 12(c) and 12(d)].

Data treatments for Figs. 12 and 13 are summarized in Fig. 14; there we compute azimuthal [Figs. 14(a) and 14(c)] and averaged radial [Figs. 14(b) and 14(d)] profiles of the density field $\rho(r,\theta,t)$. Azimuthal distributions ρ_A do not reveal any angular dependence for the steady-state regime [continuous curves in Figs. 14(a) and 14(c)], except of an insignificant statistical noise, i.e., corresponding Monte Carlo patterns [Figs. 12(a), 13(a), and 13(b)] are isotropic.[5] In fractal regions, the radial profile $\overline{\rho_R}$ obeys a power-law relation [dot curve in Fig. 14(b)]

$$\overline{\rho_R}(r) \propto r^{d_f-2}, \tag{25}$$

where the value $d_f=(1.7\pm0.05)$ calculated, the fractal dimension, is the same as measured experimentally for natural viscous fingers in radial Hele-Shaw cells [53,54].

VI. MEAN-FIELD EQUATIONS

Following our research plan, in this section, we proceed from the quasicontinuum DLA model to a deterministic mean-field theory, the purely continuum formulation. For that purpose, we need to substitute a relevant differential law in the Boltzmann kinetic terms [Eq. (9)] for Monte Carlo growth algorithms.

Fortunately, such discrete-continuum transition has already been realized phenomenologically in the previous section when we discussed the length scale origin in the quasicontinuum DLA—one may substitute the Laplacian for the average density field in a lattice neighborhood [Eq. (17)]. Thus, a deterministic analog of Eq. (14), the functional operator $\hat{F}$ in Eq. (8), is obtained as

$$\frac{\partial \rho(\mathbf{r},t)}{\partial t} = u(\mathbf{r},t)\langle \rho(\mathbf{r},t) + \delta^2 \nabla^2 \rho(\mathbf{r},t)\rangle^2, \tag{26}$$

where δ is a length microscale. This kinetic relation couples with Eq. (7), to provide a mass conservation in the finger/nutrient system. Surprisingly, the mean-field equations introduced coincide closely with the ones originally proposed by Witten and Sander [62]; we have only changed the kinetic law exponent from one to two.

[5]The growth of isotropic patterns on the anisotropic (square) grid appears to be an encouraging result: the quasicontinuum DLA model does not ''feel'' the underlying lattice, in contrast to the regular Witten-Sander DLA [62] and its miscellaneous modifications [63]; this will be analyzed in Secs. VI and VII in more detail.

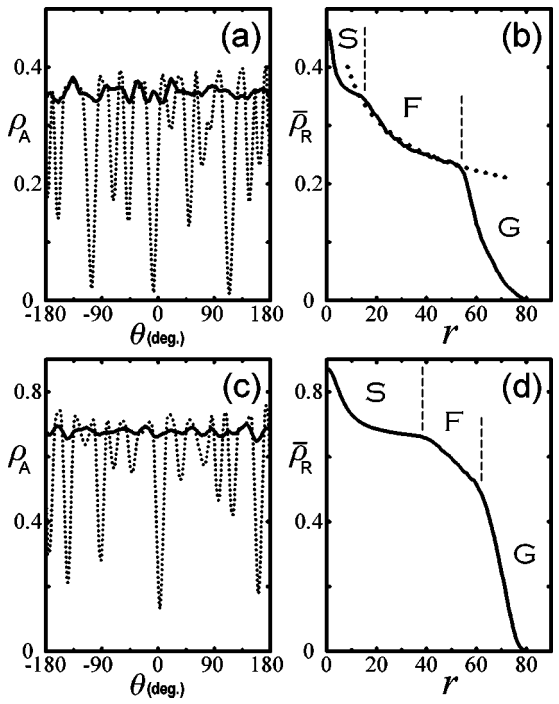

FIG. 14. Data treatments for Figs. 12 [plots (a) and (b)] and 13 [plots (c) and (d)]. (a) and (c) Azimuthal profiles, $\rho_A(\theta,t)\equiv\rho(r=r^*,\theta,t)$, in steady-state sections (continuous curves), $r^*=10a$ and $25a$ for plots (a) and (c), respectively, and in unstable sections (dot curves), $r^*=20a$ and $50a$ for plots (a) and (c), respectively. (b) and (d) Averaged radial profiles, $\overline{\rho_R}(r)\equiv(1/2\pi)\int_{-\pi}^{\pi}\rho(r,\theta)d\theta$, for patterns of a maximal gyration radius, $r_g=80a$, plots (b) and (d) for Figs. 12(d) and 13(d), respectively; here, we mark different spatial regions separated by vertical dash lines as *"S"* (steady-state front propagation), *"F"* (fractal growth), and *"G"* (gyration zone); a dot curve in plot (b) represents a power-law relation $\overline{\rho_R}(r)\propto r^{d_f-2}$ with $d_f=1.7$. Angle θ is measured in respect to an x-positive ray ($y=0$, $x>0$) in counterclockwise direction.

A. 1D planar configuration

In order to investigate general properties of the mean-field equations (7) and (26), let us consider first the problem of a one-dimensional (1D) planar displacement. Physically, this is related to a narrow rectilinear Hele-Shaw cell as its width W is an infinitesimal value in comparison with the capillary length l_c; then a liquid-liquid interface is stable, and the less viscous liquid recedes the most viscous one with a constant rate.

To formulate this 1D planar problem, we reduce the radius vector $\mathbf{r}$ in Eqs. (7) and (26) to a single coordinate (x); then bulk equations are

$$\frac{\partial\rho}{\partial t}=\frac{\partial^2 u}{\partial x^2}, \tag{27}$$

$$\frac{\partial\rho}{\partial t}=u\left\langle\rho+\delta^2\frac{\partial^2\rho}{\partial x^2}\right\rangle^2. \tag{28}$$

We define the finger $[\rho(x,t)]$ and nutrient $[u(x,t)]$ fields at $x>0$ whereas the origin $x=0$ is a growth nucleus,

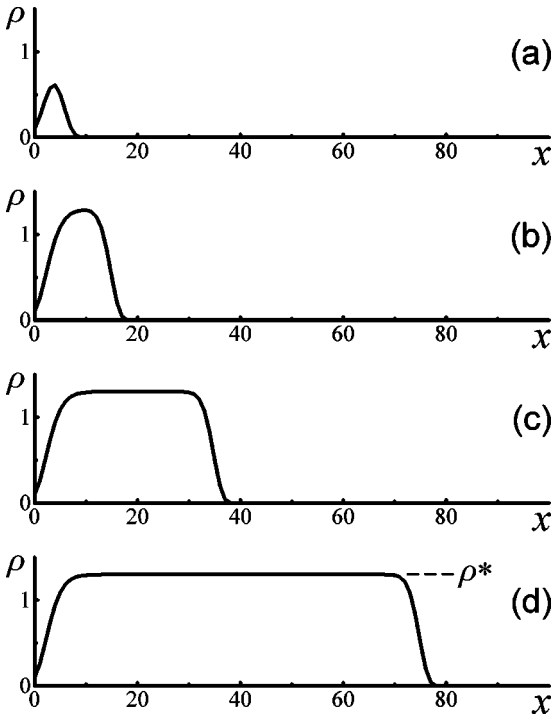

FIG. 15. Deterministic mean-field DLA in a 1D planar configuration [Eqs. (27)–(30)] ($\delta=1$, $\rho_0=0.1$). We present successive pictures [plots (a), (b), (c), and (d)] for a finger density field $\rho(x,t)$ as time t increases; ρ^* marks a stationary solution as $t\to\infty$.

$$\rho|_{x=0}=\rho_0, \quad u|_{x=0}=0. \tag{29}$$

For the formulation to be specified completely, we put the finger density to zero and fix a nutrient flux at infinity,

$$\rho|_{x\to\infty}=0, \quad \left.\frac{\partial u}{\partial x}\right|_{x\to\infty}=u_0. \tag{30}$$

Numerical studies of the 1D planar problem reveal the following: (i) solutions $\rho(x,t)$ and $u(x,t)$ are stable absolutely for all δ values and over the whole range of a parametric set (ρ_0,u_0); (ii) the finger growth dynamics does not depend on the nutrient flux at infinity u_0; in a stationary stage, nor does the dynamics depend on the initial density ρ_0; (iii) after initial transients, the finger field $\rho(x,t)$ has a sharp steplike profile, which propagates with a constant velocity. Thus, we conclude 1D planar fingers to represent a soliton family.

This solitonic behavior is illustrated in Fig. 15; there we show a time development of the finger field $\rho(x,t)$ modeled by Eqs. (27)–(30) with $\delta=1$. Starting from the nucleus $\rho=\rho_0$, first there is a stage of initial transients as the finger density approaches an eigenvalue ρ^* [Figs. 15(a) and 15(b)]. After that a stationary stage emerges [Figs. 15(c) and 15(d)]; the spatial region related ($\rho\simeq\rho^*$) expands steadily in the x-positive direction whereas a falloff shape at the finger front is time independent. So, the stationary dynamics reproduces qualitatively a natural 1D viscous displacement as one associates the liquid-liquid interface $\Gamma(t)$ with the condition $\rho=\rho^*/2$ [Eq. (6)].

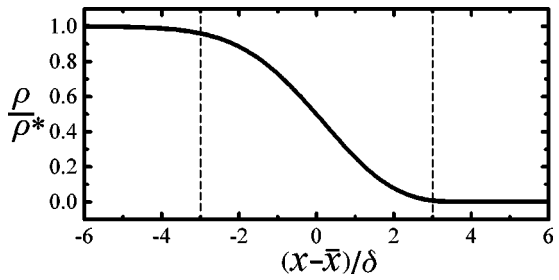

FIG. 16. Finger front region $\rho(z)=\rho(x-\bar{x})$ by Eq. (31) for deterministic mean-field DLA in a 1D planar configuration (see Fig. 15). We plot normalized finger density ρ/ρ^* as a function of $(x-\bar{x})/\delta$ where $\bar{x}$ denotes a front median, $\rho(\bar{x})=\rho^*/2$; the δ-boundary layer, $x\in(\bar{x}-3\delta,\ldots,\bar{x}+3\delta)$, is marked by vertical dash lines.

Then, let us analyze in detail the finger front, a kinetic length scale over which the density function ρ varies between ρ^* and zero; the relevant eigenequation is derived as (see Appendix C)

$$(\rho-\rho^*)(\rho+\delta^2\rho'')^3=\rho''(\rho+\delta^2\rho'')-2\rho'(\rho'+\delta^2\rho'''), \tag{31}$$

where the function ρ and its derivatives ρ', ρ'', and ρ''' are determined in respect to a variable $z\equiv x-vt$ ($v=\text{const}$ is a front velocity). The finger falloff shape calculated from that eigenequation is presented in Fig. 16. As seen from the figure, the front intermediate includes mostly a 3δ neighborhood of a median, $x\in(\bar{x}-3\delta,\ldots,\bar{x}+3\delta)$: the finger density varies there by $\approx 94\%$ of ρ^*; later we will refer to this intermediate region as "the δ-boundary layer."[6]

B. 1D radial configuration

The next deterministic problem we consider is a 1D radial displacement when the mean-field equations (7) and (26) are reduced again to a single spatial coordinate, the radius r. While this configuration does not have any natural equivalent, its investigation is necessary for the subsequent consideration of two-dimensional problems such as channel and sector ones.

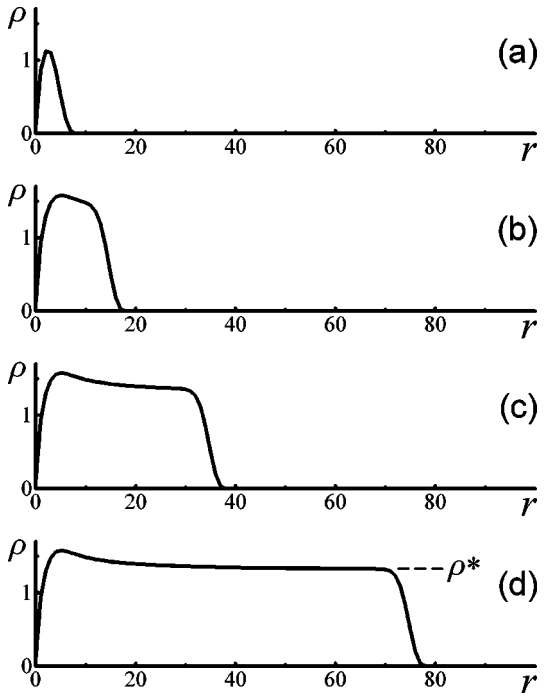

FIG. 17. Deterministic mean-field DLA in a 1D radial configuration [Eqs. (32)–(35)] ($\delta=1$, $\rho_0=0.1$). We present successive pictures [plots (a), (b), (c), and (d)] for a finger density field $\rho(r,t)$ as time t increases; ρ^* marks a quasistationary solution as $t\to\infty$.

Assuming only a radial dependence in Eqs. (7) and (26) written in polar coordinates (r,θ), we obtain bulk equations as

$$\frac{\partial\rho}{\partial t}=\frac{\partial^2 u}{\partial r^2}+\frac{1}{r}\frac{\partial u}{\partial r}, \tag{32}$$

$$\frac{\partial\rho}{\partial t}=u\left\langle \rho+\delta^2\left(\frac{\partial^2\rho}{\partial r^2}+\frac{1}{r}\frac{\partial\rho}{\partial r}\right)\right\rangle^2. \tag{33}$$

We define the finger $[\rho(r,t)]$ and nutrient $[u(r,t)]$ fields at $r>0$, whereas the origin $r\to 0$ is a growth nucleus,

$$\rho|_{r\to 0}=\rho_0, \quad u|_{r\to 0}=0. \tag{34}$$

Conditions at infinity imposed are

$$\rho|_{r\to\infty}=0, \quad r\frac{\partial u}{\partial r}\bigg|_{r\to\infty}=u_0. \tag{35}$$

Similar to the planar configuration, numerical studies reveal solutions of the 1D radial problem, $\rho(r,t)$ and $u(r,t)$, to be stable absolutely[7] for all δ values and over whole range of parameters ρ_0 and u_0; besides, the finger growth dynamics depends neither on the nutrient flux at infinity u_0 nor on the

[6]Although the finger density function $\rho(\mathbf{r},t)$ is associated with a material density throughout the paper (see, e.g., footnote 2), one should nevertheless avoid a complete equivalency. In fact, the material density of a liquid drops to zero at its boundary in a jump way, whereas the density function $\rho(\mathbf{r},t)$, a mathematical approximation, varies continuously (see Figs. 5, 9, and 15). So the intermediate at the finger front, the δ-boundary layer (see Fig. 16), should not be understood as a region where two liquids dissolve (or mix) in each other over a diffusion length scale δ, i.e., as if the process of a miscible viscous fingering was modeled. Instead, existence of the δ-boundary layer is just a consequence of the continuity of $\rho(\mathbf{r},t)$ and $u(\mathbf{r},t)$ functions; physically the microscale δ is responsible for a stability of two-dimensional solutions, as will be clarified in Sec. VI E.

[7]This does not automatically imply the absolute stability for a radial configuration in two spatial dimensions, for which one has to consider also θ perturbations neglected here.

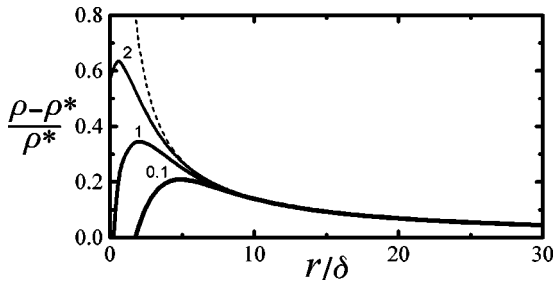

FIG. 18. $(1/r)$ singularity for deterministic mean-field DLA in a 1D radial configuration (see Fig. 17). We plot normalized density increments $(\rho-\rho^*)/\rho^*$ as functions of r/δ for different initial conditions: $\rho_0=0.1$, 1, and 2 (continuous curves with ρ_0 values shown at); a dash curve represents an asymptotic dependence $(\rho-\rho^*)/\rho^* \propto \delta/r$.

initial density ρ_0 in a quasistationary stage. Far from the origin, the quasistationary finger density approaches the same eigenvalue ρ^* and the finger field $\rho(r,t)$ has the same steplike time-independent profile as in the 1D planar problem (Fig. 15). The only difference is related to the region of small radii, $r \lesssim 10\delta$, where a $(1/r)$ singularity of the Laplacian [in Eqs. (32) and (33)] yields a density increment. This behavior is illustrated in Fig. 17 which shows a time development of the finger field $\rho(r,t)$ modeled by Eqs. (32)–(35) with $\delta=1$. Relevant structure of the $(1/r)$ singularity is presented in Fig. 18; as the initial density ρ_0 increases, that singularity increments (continuous curves) converge to the asymptotics (dash curve)

$$\frac{\rho-\rho^*}{\rho^*} \propto \frac{\delta}{r}. \tag{36}$$

C. Channel configuration

After preliminary studies of the deterministic mean-field DLA in 1D geometry, let us advance to two spatial dimensions and examine our theory for the classic Saffman-Taylor configuration of a long linear channel [15], which has been already investigated by statistical methods in Sec. V A (Figs. 1–5).

To formulate the channel problem, we consider a rectilinear (x,y) Hele-Shaw cell of width W; then bulk equations for the finger $[\rho(x,y,t)]$ and nutrient $[u(x,y,t)]$ fields are

$$\frac{\partial \rho}{\partial t} = \frac{\partial^2 u}{\partial x^2} + \frac{\partial^2 u}{\partial y^2}, \tag{37}$$

$$\frac{\partial \rho}{\partial t} = u \left\langle \rho + \delta^2 \left(\frac{\partial^2 \rho}{\partial x^2} + \frac{\partial^2 \rho}{\partial y^2} \right) \right\rangle^2. \tag{38}$$

We locate a growth nucleus at the origin,

$$\rho|_{x=y=0} = \rho_0, \quad u|_{x=y=0} = 0. \tag{39}$$

On lateral walls $y = \pm W/2$, we impose the Neuman condition (a spatial restriction) for the finger field ρ, and the Dirichlet

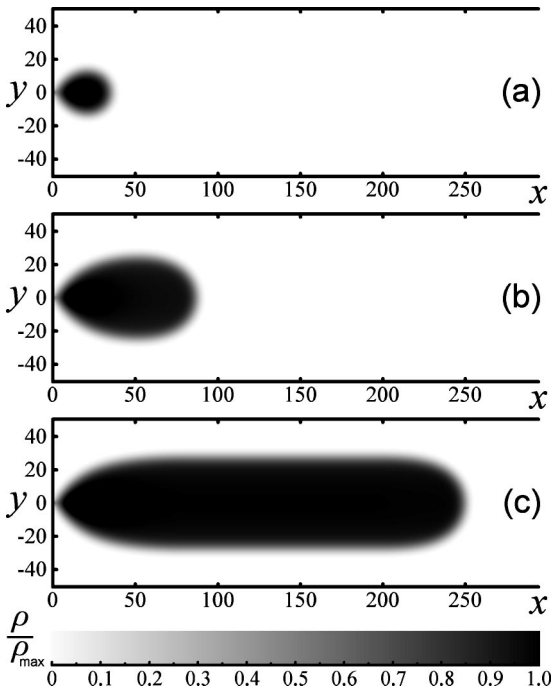

FIG. 19. Deterministic mean-field DLA in a channel configuration [Eqs. (37)–(41)] ($W=100$, $\delta=2$, an analog of Fig. 4). We present different stages of a steady-state front propagation: (a) nucleation, (b) tip formation, and (c) stationary growth.

condition (a deterministic analog of the normal reflection for wandering walkers in the quasicontinuum DLA model) for the nutrient field u,

$$\rho|_{y=\pm W/2} = 0, \quad \left.\frac{\partial u}{\partial y}\right|_{y=\pm W/2} = 0. \tag{40}$$

At infinity, we put the finger density to zero and fix the nutrient flux,

$$\rho|_{x\to\infty} = 0, \quad \left.\frac{\partial u}{\partial x}\right|_{x\to\infty} = u_0. \tag{41}$$

In order to provide an illustrative correspondence to Monte Carlo results obtained by the quasicontinuum DLA simulation for a steady-state growth regime (Figs. 4 and 5), we take the same input parameters for numerical modeling by Eqs. (37)–(41) as in Fig. 4, i.e., the channel width $W=100$ and the microscale $\delta=2$. In Figs. 19 and 20, we show a time development of the finger field $\rho(x,y,t)$ and summarize data treatments, respectively. On a basis of the 1D problems studied before, one would comment longitudinal [Fig. 20(a)] and transverse [Fig. 20(b)] profiles computed as follows. A "kink" region on the longitudinal profiles ρ_L at small x values is due to the $(1/r)$ singularity (see Fig. 18) as the finger field is in a nucleation stage [Fig. 19(a)], when a radial approximation is valid. In a stationary stage [Fig. 19(c)], the finger field propagates through the channel with a constant velocity whereas a time-independent falloff shape of the relevant longitudinal profile [continuous curve in Fig. 20(a)] obeys Eq. (31); hence the longitudinal front region

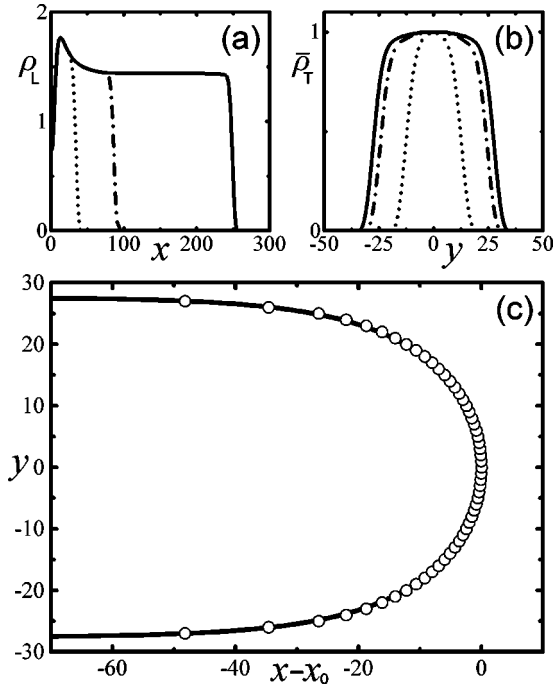

FIG. 20. Data treatments for Fig. 19. (a) Longitudinal profiles, $\rho_L(x,t) \equiv \rho(x, y=0, t)$, for Fig. 19(a) (dot curve), Fig. 19(b) (dot-dash curve), and Fig. 19(c) (continuous curve). (b) Normalized transverse profiles, $\overline{\rho_T}(y,t) \equiv \rho(x^*, y, t)/\rho(x^*, y=0, t)$, in sections of a maximal finger width, $x=x^*$, for Fig. 19(a) (dot curve), Fig. 19(b) (dot-dash curve), and Fig. 19(c) (continuous curve). (c) Contour plot of a mean density at finger tip (open circles) for a stationary growth stage [see Fig. 19(c)], compared with the Saffman-Taylor analytical solution by Eq. (21) (continuous curve) as $\lambda = 0.554$.

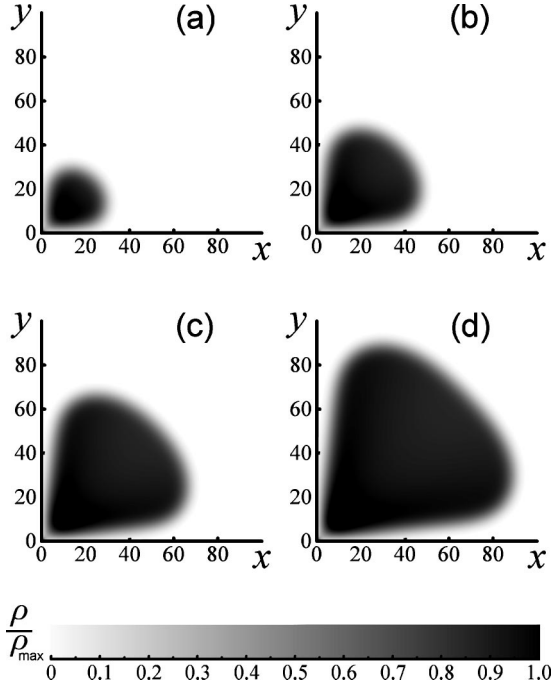

FIG. 21. Deterministic mean-field DLA in a sector configuration [Eqs. (42)–(46)] ($\theta_0 = 90°$, $\delta = 2$, an analog of Fig. 8). We present successive pictures of a steady-state front propagation as a finger gyration radius increases: $r_g = 40$, 60, 80, and 100 for plots (a), (b), (c), and (d), respectively.

represents the δ-boundary layer (see Fig. 16). Similar δ-boundary layers are formed at falloffs of a stationary transverse profile $\overline{\rho_T}$ [continuous curve in Fig. 20(b)] so this profile will converge to a step function as the microscale δ goes to zero (see footnote 2).

Comparing the Monte Carlo and numerical results between each other (Figs. 4 and 19, 5 and 20), one can resolve corresponding shapes, profiles, and mean contours to differ just insignificantly, by a statistical noise; therefore, the quasicontinuum DLA and its deterministic analog coincide asymptotically as $K \to \infty$. Remarkably, both the stochastic and deterministic models simulate a steady-state Saffman-Taylor finger [see contour plots in Figs. 5(c) and 20(c)]; thus, we conclude our formulation, Eqs. (37)–(41), to be a valid equivalent of the classic Saffman-Taylor hydrodynamics [15].

D. Sector configuration

Finally, let us apply the deterministic mean-field DLA for the other important case in two spatial dimensions, the sector configuration, in order to establish a connection to Monte Carlo results presented in Sec. V B (Figs. 6–11).

To formulate the sector problem, we consider an angular Hele-Shaw cell [50] and switch the Cartesian relations (37)–(41) to polar coordinates (r, θ); then bulk equations for the finger $[\rho(r,\theta,t)]$ and nutrient $[u(r,\theta,t)]$ fields are

$$\frac{\partial \rho}{\partial t} = \frac{\partial^2 u}{\partial r^2} + \frac{1}{r}\frac{\partial u}{\partial r} + \frac{1}{r^2}\frac{\partial^2 u}{\partial \theta^2}, \tag{42}$$

$$\frac{\partial \rho}{\partial t} = u\left\langle \rho + \delta^2\left(\frac{\partial^2 \rho}{\partial r^2} + \frac{1}{r}\frac{\partial \rho}{\partial r} + \frac{1}{r^2}\frac{\partial^2 \rho}{\partial \theta^2}\right)\right\rangle^2. \tag{43}$$

Locating a growth nucleus at the origin, we set

$$\rho|_{r\to 0} = \rho_0, \quad u|_{r\to 0} = 0. \tag{44}$$

On sector walls, $\theta = \pm \theta_0/2$, we impose the Neuman condition for the finger field ρ, and the Dirichlet condition for the nutrient field u (vector $\mathbf{n}$ denotes the unit normal to a wall),

$$\rho|_{\theta=\pm\theta_0/2} = 0, \quad (\mathbf{n}\cdot\nabla u)|_{\theta=\pm\theta_0/2} = 0. \tag{45}$$

As in Eqs. (41), we put the finger density to zero and fix the nutrient flux at infinity,

$$\rho|_{r\to\infty} = 0, \quad r\left.\frac{\partial u}{\partial r}\right|_{r\to\infty} = u_0. \tag{46}$$

For numerical modeling, we take the sector of right angle, $\theta_0 = 90°$, which has been already investigated by statistical methods. In Figs. 21 and 22, we show a time development of the finger field $\rho(r,\theta,t)$ and summarize data treatments, respectively. Similar to the channel configuration, one would

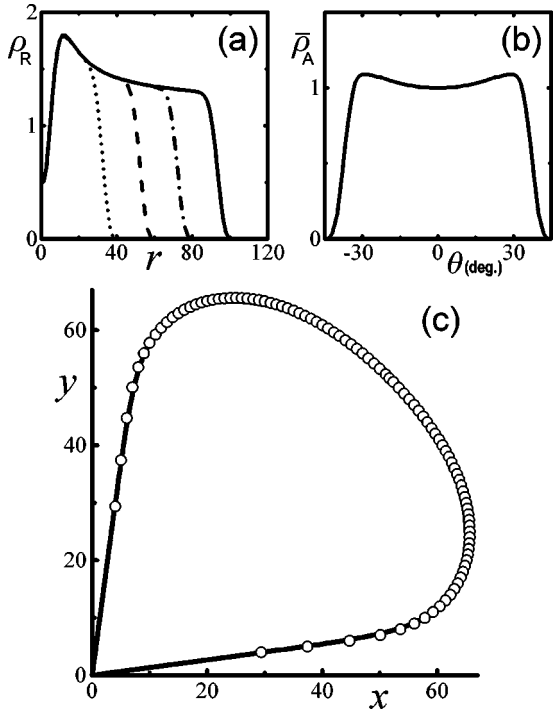

FIG. 22. Data treatments for Fig. 21. (a) Radial profiles, $\rho_R(r,t)\equiv\rho(r,\theta=0°,t)$, for Fig. 21(a) (dot curve), Fig. 21(b) (dash curve), Fig. 21(c) (dot-dash curve), and Fig. 21(d) (continuous curve). (b) Normalized azimuthal profile, $\overline{\rho_A}(\theta)\equiv\rho(r^*,\theta)/\rho(r^*,\theta=0°)$, in a quasistationary section, $r^*=50$, for Fig. 21(c). (c) Contour plot of a mean density (open circles) for a finger of gyration radius $r_g=80$ [see Fig. 21(c)], compared with the Saffman-Taylor conformal transformation by Eqs. (A2) and (A3) (continuous curve) as $\lambda_\theta=0.81$.

comment radial [Fig. 22(a)] and azimuthal [Fig. 22(b)] profiles computed as follows. On the radial profiles ρ_R, a ''kink'' region at small r values and subsequent smooth decrease of the finger density to a quasistationary eigenvalue are due to the $(1/r)$ singularity in Eqs. (42) and (43), as in the 1D radial problem (see Figs. 17 and 18). Both quasistationary radial and azimuthal profiles obey Eq. (31) at their falloffs where δ-boundary layers are therefore formed (see Fig. 16). A bimodal behavior of the azimuthal profile $\overline{\rho_A}$, the local minimum at $\theta=0°$, is caused by a secondary $(1/r)$ singularity, which takes place close to sector walls; since that singularity increments are directly proportional to δ [Eq. (36)], this bimodal profile will converge to a step function as the microscale δ goes to zero (see footnote 2).

As in the channel configuration, the finger shape (Fig. 21) together with its mean contour and profiles (Fig. 22) look like counterparts of corresponding Monte Carlo results (Figs. 8 and 9, respectively) obtained by the quasicontinuum DLA simulation for a steady-state growth regime, with only insignificant discrepancy by a statistical noise. This yields one more verification for an asymptotic coincidence of the stochastic and deterministic models; also we conclude the quasicontinuum DLA algorithm to simulate actually isotropic patterns [first it was noticed and discussed in Sec. V C]—the on-square-lattice data in Fig. 9 coincide with the off-lattice ones in Fig. 22. Besides, the contour plot of a mean finger density [Fig. 22(c)] follows precisely the relevant Saffman-Taylor conformal transformation [Eqs. (A2) and (A3)] with $\lambda_\theta=0.81$ as for the quasicontinuum DLA [Fig. 9(c)], so the conformal extension proposed is justified by the deterministic mean-field theory as well.

E. Stability of two-dimensional solutions

Numerical investigations of the mean-field equations (7) and (26) in channels and sectors report, among others, a rather surprising conclusion: there exists a stability length scale so that two-dimensional solutions are steady-state only within such scale. Thus, our deterministic continuum theory seems to keep basic properties of its stochastic quasicontinuum framework, i.e., a stable behavior within the capillary length l_c and then a developing destabilization on larger scales (see, e.g., Figs. 3, 7, and 13).

As a matter of fact, this seeming paradox may be understood and explained qualitatively as follows. While the mean-field determinism gives us an opportunity to derive an ''ideal'' solution, in numerical modeling, however, one has to consider unavoidable residual errors, which emerge due to two reasons: (i) a discrete numerical scheme being applied substitutes finite ratios for derivatives so errors of an inconsistency appear, and (ii) all intermediate calculations produce a random computational noise, the analog of a statistical one.[8] Hence, the large-scale instability origin in Eqs. (7) and (26), the noise and errors, is the same as in the quasicontinuum DLA simulation, only mechanisms related are different: either statistical or numerical.

A detailed stability analysis reveals the δ-boundary layer (Fig. 16) to be the very region responsible for a damping of statistical or numerical perturbations; its damping capacity is proportional to δ, i.e., the capillary length $l_c\propto\delta$ may be introduced to the deterministic mean-field theory as well.[9] Quantitatively, a noise amplitude needed to drive two-

[8]In a computer representation, variables and constants are recorded with a fixed accuracy; so each elementary operation such as addition, subtraction, multiplication, division, raising to a power, etc., deals with the necessity to round resulting numbers.

[9]This introduction of the capillary length scale l_c, a function of numerical noise and errors, raises an asymptotic selection problem as follows. The capillary length l_c is responsible, except for a two-dimensional stability, principally for the selection of a physical solution among a mathematically possible one-parameter family; corresponding parameters are the relative finger width λ [Eq. (21)] and the relative angular width λ_θ [Eq. (A1)] in channel and sector configurations, respectively. At small l_c values, λ approaches 1/2 whereas λ_θ obeys Eq. (24); the increase of l_c yields increments to both λ and λ_θ, depending on l_c in a power-law way [22–24]. The parameters λ and λ_θ selected should therefore increase substantially as one removes numerical noise and errors from the mean-field equations. So which two-dimensional solutions are modeled by Eqs. (7) and (26) in a zero-noise limit? Unfortunately, such asymptotic selection problem is obscure since it requires pure analytical methods being just in a development stage. We expect to clarify this point in a forthcoming publication.

dimensional solutions unstable vanish exponentially as the microscale δ decreases, making a phenomenological counterpart with the dependence $l_c(K) \propto \log K$ [Eq. (16)] derived statistically for the quasicontinuum DLA model (see Fig. 2). Thus, stability properties of our solutions reproduce the ones for the Saffman-Taylor hydrodynamics in case of a finite surface tension [17–21]; similarly, that hydrodynamic solutions are characterized by a finite-amplitude nonlinear instability whose threshold decreases as an exponential function of the surface tension coefficient d_0,[10] the squared dimensionless ratio of the capillary length l_c to a macroscale imposed externally (e.g., the width W of a rectilinear Hele-Shaw cell).

VII. DISCUSSION

To review principal results obtained in the two previous sections, we have comprehensively investigated the quasicontinuum DLA model (Sec. V) and its deterministic mean-field analog (Sec. VI) for various spatial configurations in two dimensions such as channel, sector, and radial ones. Monte Carlo patterns simulated by the quasicontinuum DLA demonstrate a striking resemblance to natural Hele-Shaw structures (see Figs. 1, 3, 4, 6, 7, 8, 10, 12, and 13) and, a remarkable achievement, follow precisely the Saffman-Taylor analytical solutions for steady-state growth regimes (see Figs. 5 and 9). This allows us to conclude the relevant deterministic mean-field formulation introduced, Eqs. (7) and (26), to be a valid density equivalent of the classic Saffman-Taylor hydrodynamics, Eqs. (1)–(4), in terms of the liquid-liquid interface evolution $\Gamma(t)$ [Eq. (6)] (see Figs. 19–22). Nevertheless, one important question still remains open: is our mean-field theory the only true or, maybe, there exists an extended family of possible theories?

In order to clarify the question posed, one has to come back to the beginning of our stochastic framework (Sec. IV) where a kinetic hypothesis on the two-particle interaction intensity has been suggested [Eq. (13)]. There we assumed that interaction intensity $w(\mathbf{r},t)$ to be a linear function of neighboring density field; however, any power-law dependence

$$w(\mathbf{r},t) = \left\langle \sum_i \rho(\mathbf{r}+\mathbf{e}_i,t) \right\rangle^{\alpha} \tag{47}$$

with an exponent $\alpha > 0$ satisfies the required conditions of (i) neighborhood equivalency, (ii) growth threshold, and (iii) isometric invariance as well as the linear connection fixed by Eq. (13), so why do we emphasize the point $\alpha = 1$? This needs a detailed investigation.[11]

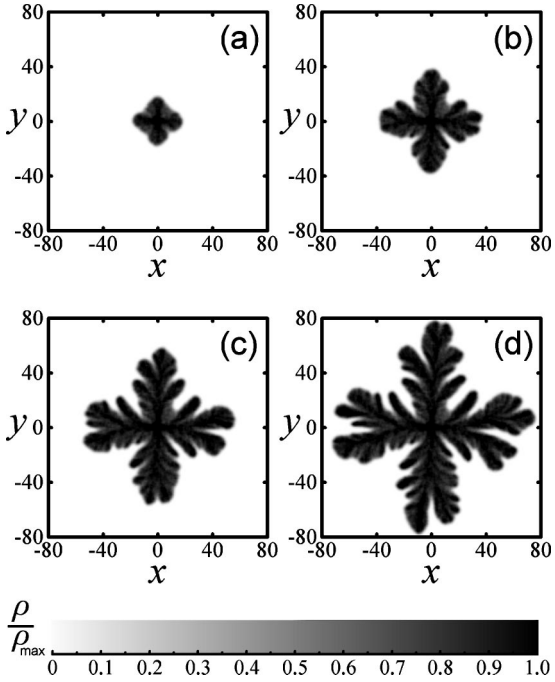

FIG. 23. α-extended quasicontinuum DLA simulation on a square grid (x,y) of spacing $a=1$ in a radial configuration. Aggregation probability $P(x,y,t)$ is set by Eq. (48) with $\alpha = 1/2$; discreteness $K = 2^{12}$. We present successive pictures as a gyration radius increases: $r_g = 20a$, $40a$, $60a$, and $80a$ for plots (a), (b), (c), and (d), respectively.

Testing the α-extended quasicontinuum DLA model [Eq. (47)], we apply corresponding Monte Carlo algorithms for a two-dimensional radial configuration. Similar to statistical studies in case of $\alpha = 1$ [see Figs. 12 and 13 in Sec. V C], we take a square grid $\mathbf{r} = (x,y)$ of spacing a on which the aggregation probability $P(x,y,t)$ formula is modified from Eq. (15) to its α variant,

$$P(x,y,t) = \langle \rho(x+a,y,t) + \rho(x-a,y,t) + \rho(x,y+a,t) + \rho(x,y-a,t) \rangle^{\alpha+1}. \tag{48}$$

Simulations by Eq. (48) for different α values report a drastic influence of the underlying lattice on resulting shapes: there definitely appear preferential growth directions if $\alpha \neq 1$. As one can resolve from Figs. 23 ($\alpha = 1/2$) and 24 [$\alpha = 1(1/2)$], Monte Carlo patterns with $\alpha < 1$ are oriented along the x and y axes whereas the choice of $\alpha > 1$ leads to the xy diagonal orientation. While this lattice effect noticed, in itself, is not surprising for DLA-based algorithms, which usually produce strongly anisotropic clusters,[12] it settles serious arguments to disprove a capability of the α-extended quasicontinuum DLA to simulate the viscous fingering in regular Hele-Shaw cells. Indeed, our mean-field theory is

[10] Related results from a structural stability analysis and numerical studies, compared with experimental data, are summarized in Figs. 3, 6, and 7 of Ref. [21].

[11] It would be better, undoubtedly, to consider a more general dependence $w = w(\rho)$ than given by Eq. (47); nevertheless, our restriction is adequate since the power-law family chosen represents a complete functional cover of possible formulations (in terms of the Taylor polynomial decomposition).

[12] For a comprehensive analysis of reasons why the cluster anisotropy systematically appears in on-lattice DLA simulations, see Refs. [83,115–120].

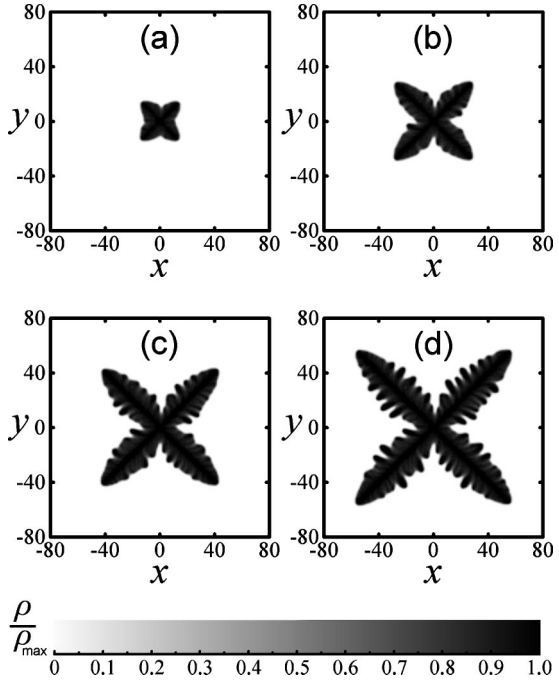

FIG. 24. α-extended quasicontinuum DLA simulation on a square grid (x,y) of spacing $a=1$ in a radial configuration. Aggregation probability $P(x,y,t)$ is set by Eq. (48) with $\alpha=1(1/2)$; discreteness $K=2^{12}$. We present successive pictures as a gyration radius increases: $r_g=20a$, $40a$, $60a$, and $80a$ for plots (a), (b), (c), and (d), respectively.

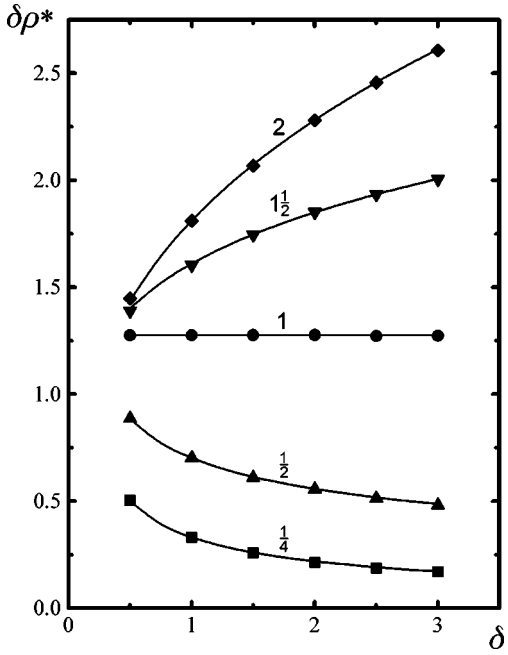

FIG. 25. Product $(\delta\rho^*)$ as a function of microscale δ for α-extended deterministic mean-field DLA in a 1D planar configuration [Eqs. (27)–(30) where Eq. (49) substitutes for Eq. (28)]. We plot numerical results for $\alpha=1/4$ (bars), 1/2 (up triangles), 1 (circles), 1(1/2) (down triangles), and 2 (diamonds); corresponding continuous curves (with α values shown at) represent a theoretical relation $\rho^*\propto\delta^{-2/(\alpha+1)}$.

aimed to describe a viscous liquid flow as isotropic,[13] the result achieved only with $\alpha=1$ when off-lattice circular shapes grow in the radial configuration (Figs. 12 and 13).

Although statistical studies of the α-extended quasicontinuum DLA model are rather illustrative, they provide just a qualitative test. For further theoretical clarifications, one has to examine corresponding mean-field equations that are Eq. (7) coupled with the α variant of Eq. (26),

$$\frac{\partial\rho(\mathbf{r},t)}{\partial t}=u(\mathbf{r},t)\langle\rho(\mathbf{r},t)+\delta^2\nabla^2\rho(\mathbf{r},t)\rangle^{\alpha+1}. \qquad (49)$$

It is obvious that steady-state deterministic solutions $\rho(\mathbf{r},t)$ and $u(\mathbf{r},t)$ cannot depend on features of a numerical scheme being applied, since there should be no correlation between the structure of a numerical grid and the spatial symmetry of a deterministic problem. Hence, the previous lattice arguments concerning the anisotropy of resulting shapes are inappropriate here,[14] so we need to derive a more fundamental criterion than the isotropy/anisotropy to justify the specific case $\alpha=1$.

In order to catch a key aspect of that criterion, let us consider the stationary finger density ρ^* as a function of the microscale δ and the exponent α; the relevant eigenequation, the α variant of Eq. (31), is written as

$$(\rho-\rho^*)(\rho+\delta^2\rho'')^{\alpha+2}=\rho''(\rho+\delta^2\rho'')-(\alpha+1)\rho'(\rho'+\delta^2\rho'''). \qquad (50)$$

Its trivial dimensional analysis reveals the following relation (see Fig. 25 for numerical results in the 1D planar configuration):

$$\rho^*\propto\delta^{-2/(\alpha+1)}, \qquad (51)$$

which yields a length-density conservation

$$\delta\rho^*=\text{const as } \alpha=1. \qquad (52)$$

For a propagating finger field $\rho(\mathbf{r},t)$, physical sense of the $(\delta\rho^*)$ conservation becomes clear as one reminds the issue of a front intermediate, the δ-boundary layer (Fig. 16). The microscale δ multiplied by the eigenvalue ρ^* estimates a layer volume, which is inversely proportional to the propa-

[13]In principle, natural examples of anisotropic viscous morphologies are widely known [121–132]; all these experimental structures, however, are related to physical systems where the anisotropy is either superimposed (e.g., by specific configurations of Hele-Shaw cells) or introduced as an internal property of the viscous liquid itself (e.g., in experiments with liquid crystals). None of the complex factors mentioned above is considered in the model so one could expect to simulate regular isotropic patterns by Eq. (48) [premise (iii) in Sec. IV].

[14]The isotropic Laplacian-type function $(\rho+\delta^2\nabla^2\rho)$ in Eq. (49) raised to any power $(\alpha+1)$ will preserve its isotropy.

gation velocity $\partial\Gamma/\partial t$ of the finger being a solitonic wave. As a consequence, the $(\delta\rho^*)$ conservation for $\alpha=1$ implies the finger growth rate to be a constant at variations of δ,[15] i.e., the interface dynamics $\Gamma(t)$ is determined principally by external conditions whereas the microscale δ represents an independent length parameter of the theory.[16] Thus, we conclude only the golden mean $\alpha=1$ and therefore, only the quadratic kinetic law of aggregation as given by Eq. (26), to be essentially physical, in contrast to other possible formulations that are just abstract mathematical substitutions.

VIII. CONCLUSION

The present paper's contribution to physics of nonequilibrium growth processes consists in the exploration of a universal ''density'' formalism for stochastic and deterministic modeling the immiscible viscous fingering in Hele-Shaw cells (usually referred to as the Saffman-Taylor problem). The stochastic model simulates Monte Carlo patterns, which resemble natural Hele-Shaw fingers and, for steady-state growth regimes, follow precisely the Saffman-Taylor analytical solutions in channel and sector configurations. The relevant deterministic theory, a complete set of differential equations for a time development of density fields, is proved to be equivalent to the classic Saffman-Taylor hydrodynamics in terms of an interface evolution. This advances current status of the Saffman-Taylor problem substantially, allowing us to study and describe the viscous fingering phenomena over the whole range of experimental regimes: from steady state to unstable fractal where the classic hydrodynamics fails.

ACKNOWLEDGMENTS

I would like to thank sincerely Dr. Natasha Chernova, Dr. Nikolay Andreev, Dr. Maxim Lobanov, and Miss Elena Bibik for fruitful discussions and helpful comments. I am also grateful to LTPD Computer Center (Moscow State University) for computing resources provided.

APPENDIX A: CONFORMAL TRANSFORMATION OF SAFFMAN-TAYLOR SOLUTIONS TO POLAR COORDINATES

Let us consider the classic Saffman-Taylor family of solutions, $x=x(y,x_0,\lambda,W)$ [Eq. (21)], which describes the contour of a steady-state viscous finger penetrating in a rectilinear Hele-Shaw cell [15]. As we switch to the sector configuration $r=r(\theta,r_g,\lambda_\theta,\theta_0)$, the polar angle θ multiplied by the gyration radius r_g becomes an equivalent of the ordinate y, whereas the relative angular width λ_θ and the sector angle θ_0 substitute for parameters λ and W, respectively. Then the left term in Eq. (21) $(x-x_0)$ transforms to its radial equivalent $(r-r_g)$, allowing us to derive the finger contour in polar coordinates as

$$\frac{r(\theta)-r_g}{r_g}=\frac{\theta_0(1-\lambda_\theta)}{2\pi}\ln\left[\frac{1}{2}\left(1+\cos\frac{2\pi\theta}{\lambda_\theta\theta_0}\right)\right], \quad \text{(A1)}$$

where angles θ and θ_0 are measured in radians.

Coming back to the Cartesian basis (x,y), we combine this conformal transformation with the conversion formulas by Eqs. (22); for a right sector $\theta_0=\pi/2$, one obtains

$$x(\theta)=\frac{r_g(\cos\theta-\sin\theta)}{\sqrt{2}}\left\langle 1+\frac{(1-\lambda_\theta)}{4}\ln\left[\frac{1}{2}\left(1+\cos\frac{4\theta}{\lambda_\theta}\right)\right]\right\rangle, \quad \text{(A2)}$$

$$y(\theta)=\frac{r_g(\cos\theta+\sin\theta)}{\sqrt{2}}\left\langle 1+\frac{(1-\lambda_\theta)}{4}\ln\left[\frac{1}{2}\left(1+\cos\frac{4\theta}{\lambda_\theta}\right)\right]\right\rangle, \quad \text{(A3)}$$

where $\theta\in(-(\pi/4)\lambda_\theta,\ldots,(\pi/4)\lambda_\theta)$ is used as a running variable.

APPENDIX B: RELATIVE ANGULAR WIDTH $\lambda_\theta(\theta_0)$

Let us analyze the relative angular width λ_θ of a steady-state viscous finger penetrating in a sector-shaped Hele-Shaw cell of angle $\theta_0\in(0,\ldots,2\pi)$ [50]. In order to derive the dependence $\lambda_\theta=\lambda_\theta(\theta_0)$, we consider the following:

(i) The function $\lambda_\theta(\theta_0)$ approaches 1/2 for an infinitesimally narrow sector, $\theta_0\to 0$ [31–35].

(ii) $\lambda_\theta(\theta_0)$ should yield a linear connection [Eq. (23)] for small and moderate sector angles, $\theta_0\lesssim\pi/2$ [50,85].

(iii) The limit of a radial configuration $\theta_0\to 2\pi$ predetermines the asymptotic condition $\lambda_\theta(2\pi)=1$.

To satisfy the requirements above, we propose a one-parameter family of curves,

$$\lambda_\theta(\theta_0)=\frac{1}{2}+\frac{\theta_0}{4\pi+A(\theta_0-2\pi)}, \quad \text{(B1)}$$

where $0<A<2$ is a free coefficient. The best fit of this relation to both experimental [50] and Monte Carlo (Figs. 8 and 10) data is achieved as $A=\pi/2$, yielding the function $\lambda_\theta(\theta_0)$ as given by Eq. (24).[17]

[15]The velocity balance by Eq. (52) broken in case of $\alpha\neq 1$ explains satisfactorily the anisotropy effect, which is observed for on-square-lattice patterns (Figs. 23 and 24) simulated by the α -extended quasicontinuum DLA; see Appendix D.

[16]This makes an explicit relationship with the classic Saffman-Taylor hydrodynamics, Eqs. (1)–(4); similarly, one can hardly imagine for the liquid-liquid interface velocity $\partial\Gamma/\partial t$ (imposed by external conditions in a Hele-Shaw cell) any direct dependence on the surface tension coefficient d_0 (being a material function).

[17]As a matter of fact, Eq. (B1) is not superimposed so one may introduce instead another parametric family for the fit, as well as one may find a number of reasons to criticize our choice. We do not therefore claim Eqs. (B1) and (24) to be the only true, but rather to provide an approximation.

APPENDIX C: EIGENEQUATION FOR 1D PLANAR PROBLEM

Let us consider the 1D-spatial finger density field $\rho(x,t)$ to be a solitonic wave which propagates in the x-positive direction with a constant velocity v,

$$\rho(x,t)=\rho(x-vt). \tag{C1}$$

Then we introduce a variable $z\equiv x-vt$ in order to rewrite Eqs. (27) and (28) as

$$\rho'=-\frac{u''}{v}, \tag{C2}$$

$$\rho'=-\frac{u}{v}(\rho+\delta^2\rho'')^2, \tag{C3}$$

where derivatives ρ', ρ'', and u'' are determined in respect to z.

As one sets $\rho(z)=\rho^*$ to be a stationary solution at $z\to-\infty$ (far behind the finger front), Eq. (C2) becomes integrable,

$$\rho-\rho^*=-\frac{u'}{v}. \tag{C4}$$

An expression for the term $(-u'/v)$ can be obtained independently from Eq. (C3) by its differentiation,

$$-\frac{u'}{v}=\left[\frac{\rho'}{(\rho+\delta^2\rho'')^2}\right]'. \tag{C5}$$

Finally, a combination of Eqs. (C4) and (C5) yields the eigenequation as given by Eq. (31).

APPENDIX D: ON-LATTICE ANISOTROPY FOR α-EXTENDED QUASICONTINUUM DLA MODEL

From a power-law relation by Eq. (51) between the eigenvalue ρ^* and the microscale δ, their product $(\delta\rho^*)$ is strongly dependent on δ in case of $\alpha\neq1$ (see Fig. 25). So what does it mean for an on-lattice aggregation? While the microscale δ in a given polar direction θ is calculated as the distance between two lattice sites divided by the number of jumps needed to make a path (one has to approximate a lattice line by a train of steps), an anisotropic angular dependence $\delta=\delta(\theta)$ is superimposed.[18] We should therefore observe a preferred growth in lattice directions where the function $(\delta\rho^*)$ reaches its minimum, i.e., the propagation velocity $\partial\Gamma/\partial t$ is in the maximum.

In statistical studies of the α-extended quasicontinuum DLA model (see Figs. 23 and 24), we considered nearest-neighborhood interactions for the on-square-lattice (x,y) aggregation [Eq. (48)]; hence in directions of main axes, $\langle10\rangle$, $\langle01\rangle$, $\langle\overline{1}0\rangle$, and $\langle0\overline{1}\rangle$, the microscale δ equals the lattice spacing a, whereas in diagonal directions, $\langle11\rangle$, $\langle\overline{11}\rangle$, $\langle\overline{1}\overline{1}\rangle$, and $\langle1\overline{1}\rangle$, the microscale δ equals $a/\sqrt{2}$. As a result, the preferred growth for Monte Carlo patterns of $\alpha=1/2$ (Fig. 23) and $\alpha=1(1/2)$ (Fig. 24) was observed along the x and y axes and the xy diagonals, respectively, in full agreement with the discussion above.

[18] Although this direction-dependent definition of the microscale δ is somewhat different from the one introduced in terms of a lattice Laplacian [Sec. V A], both the definitions yield similar measures.

[1] J. S. Langer, Rev. Mod. Phys. **52**, 1 (1980).
[2] B. B. Mandelbrot, *The Fractal Geometry of Nature* (Freeman, New York, 1982).
[3] J. Feder, *Fractals* (Pergamon, New York, 1988).
[4] *Growth and Form: Nonlinear Aspects*, edited by M. Ben Amar, P. Pelcé, and P. Tabeling (Plenum, New York, 1991).
[5] T. Vicsek, *Fractal Growth Phenomena*, 2nd ed. (World Scientific, Singapore, 1992).
[6] *Growth Patterns in Physical Sciences and Biology*, edited by J. M. Garcia-Ruiz, E. Louis, P. Meakin, and L. M. Sander (Plenum, New York, 1993).
[7] *Fractals in Natural Sciences*, edited by T. Vicsek, M. Shlesinger, and M. Matsushita (World Scientific, Singapore, 1994).
[8] A.-L. Barabási and H. E. Stanley, *Fractal Concepts in Surface Growth* (Cambridge University Press, Cambridge, 1995).
[9] P. Meakin, *Fractals, Scaling and Growth Far from Equilibrium* (Cambridge University Press, Cambridge, 1997).
[10] H. J. S. Hele-Shaw, Nature (London) **58**, 34 (1898).
[11] D. Bensimon, L. P. Kadanoff, S. Liang, B. I. Shraiman, and C. Tang, Rev. Mod. Phys. **58**, 977 (1986).
[12] D. A. Kessler, J. Koplik, and H. Levine, Adv. Phys. **37**, 255 (1988).
[13] *Dynamics of Curved Fronts*, edited by P. Pelcé (Academic, Orlando, 1988).
[14] K. V. McCloud and J. V. Maher, Phys. Rep. **260**, 139 (1995).
[15] P. G. Saffman and G. I. Taylor, Proc. R. Soc. London, Ser. A **245**, 312 (1958); P. G. Saffman, Q. J. Mech. Appl. Math. **12**, 146 (1959); G. I. Taylor and P. G. Saffman, *ibid.* **12**, 265 (1959).
[16] S. Richardson, J. Fluid Mech. **56**, 609 (1972); **102**, 263 (1981); Q. J. Mech. Appl. Math. **35**, 531 (1982).
[17] J. W. McLean and P. G. Saffman, J. Fluid Mech. **102**, 455 (1981); J.-M. Vanden-Broeck, Phys. Fluids **26**, 2033 (1983).
[18] G. Tryggvason and H. Aref, J. Fluid Mech. **136**, 1 (1983); **154**, 287 (1985).
[19] D. A. Kessler and H. Levine, Phys. Rev. A **32**, 1930 (1985); **33**, 2621 (1986); **33**, 2634 (1986); **33**, 3625 (1986); Phys. Fluids **30**, 1246 (1987).

[20] A. J. DeGregoria and L. W. Schwartz, Phys. Fluids **28**, 2313 (1985); L. W. Schwartz, *ibid.* **29**, 3086 (1986); A. J. DeGregoria and L. W. Schwartz, J. Fluid Mech. **164**, 383 (1986); Phys. Rev. Lett. **58**, 1742 (1987); L. W. Schwartz and A. J. DeGregoria, Phys. Rev. A **35**, 276 (1987).
[21] D. Bensimon, Phys. Rev. A **33**, 1302 (1986).
[22] B. I. Shraiman, Phys. Rev. Lett. **56**, 2028 (1986); D. Bensimon, P. Pelcé, and B. I. Shraiman, J. Phys. (Paris) **48**, 2081 (1987).
[23] D. C. Hong and J. S. Langer, Phys. Rev. Lett. **56**, 2032 (1986); Phys. Rev. A **36**, 2325 (1987).
[24] R. Combescot, T. Dombre, V. Hakim, Y. Pomeau, and A. Pumir, Phys. Rev. Lett. **56**, 2036 (1986); R. Combescot, V. Hakim, T. Dombre, Y. Pomeau, and A. Pumir, Phys. Rev. A **37**, 1270 (1988).
[25] P. G. Saffman, J. Fluid Mech. **173**, 73 (1986); IMA J. Appl. Math. **46**, 137 (1991).
[26] S. D. Howison, J. Fluid Mech. **167**, 439 (1986); SIAM (Soc. Ind. Appl. Math.) J. Appl. Math. **46**, 20 (1986); Eur. J. Appl. Math. **3**, 209 (1992); S. D. Howison and S. Richardson, *ibid.* **6**, 441 (1995).
[27] S. Tanveer, Phys. Fluids **30**, 1589 (1987); **30**, 2318 (1987); S. Tanveer and P. G. Saffman, *ibid.* **31**, 3188 (1988); S. Tanveer, Philos. Trans. R. Soc. London, Ser. A **343**, 155 (1993).
[28] L. P. Kadanoff, Phys. Rev. Lett. **65**, 2986 (1990); G. L. Vasconcelos and L. P. Kadanoff, Phys. Rev. A **44**, 6490 (1991); G. L. Vasconcelos, Phys. Rev. E **48**, R658 (1993); **58**, 6858 (1998).
[29] M. B. Mineev-Weinstein and S. P. Dawson, Phys. Rev. E **50**, R24 (1994); M. Mineev-Weinstein, Phys. Rev. Lett. **80**, 2113 (1998).
[30] F. X. Magdaleno and J. Casademunt, Phys. Rev. E **57**, R3707 (1998); **60**, R5013 (1999); J. Casademunt and F. X. Magdaleno, Phys. Rep. **337**, 1 (2000).
[31] E. A. Brener, D. A. Kessler, H. Levine, and W.-J. Rappel, Europhys. Lett. **13**, 161 (1990).
[32] M. Ben Amar, V. Hakim, M. Mashaal, and Y. Couder, Phys. Fluids A **3**, 1687 (1991); **3**, 2039(E) (1991).
[33] M. Ben Amar, Phys. Rev. A **43**, 5724 (1991); **44**, 3673 (1991).
[34] R. Combescot and M. Ben Amar, Phys. Rev. Lett. **67**, 453 (1991); R. Combescot, Phys. Rev. A **45**, 873 (1992).
[35] Y. Tu, Phys. Rev. A **44**, 1203 (1991).
[36] M. Ben Amar, Phys. Rev. E **51**, R3819 (1995).
[37] M. J. P. Gingras and Z. Rácz, Phys. Rev. A **40**, 5960 (1989).
[38] D. Jasnow and C. Yeung, Phys. Rev. E **47**, 1087 (1993); S. K. Sarkar and D. Jasnow, Pramana, J. Phys. **41**, 389 (1993).
[39] H. Power, Eng. Anal. Boundary Elem. **14**, 297 (1994); H. Hadavinia, S. G. Advani, and R. T. Fenner, *ibid.* **16**, 183 (1995).
[40] J. A. Miranda and M. Widom, Physica D **120**, 315 (1998).
[41] R. A. Wooding, J. Fluid Mech. **7**, 501 (1960); **39**, 477 (1969).
[42] E. Pitts, J. Fluid Mech. **97**, 53 (1980).
[43] C.-W. Park, S. Gorell, and G. M. Homsy, J. Fluid Mech. **141**, 275 (1984); C.-W. Park and G. M. Homsy, Phys. Fluids **28**, 1583 (1985).
[44] J. L. Marx, Science **228**, 1077 (1985).
[45] J. Walker, Sci. Am. **257**, 134 (1987).
[46] P. Tabeling, G. Zocchi, and A. Libchaber, J. Fluid Mech. **177**, 67 (1987).
[47] A. R. Kopf-Sill and G. M. Homsy, Phys. Fluids **31**, 242 (1988).
[48] T. Maxworthy, J. Fluid Mech. **177**, 207 (1987); J. Wiggert and T. Maxworthy, Phys. Rev. E **47**, 1931 (1993).
[49] Y. Couder, in *Chaos, Order and Patterns*, edited by R. Artuso, P. Cvitanovic, and G. Casati (Plenum, New York, 1991), p. 203; E. Lajeunesse and Y. Couder, J. Fluid Mech. **419**, 125 (2000).
[50] H. Thomé, M. Rabaud, V. Hakim, and Y. Couder, Phys. Fluids A **1**, 224 (1989).
[51] J. Bataille, Rev. Inst. Fr. Pet. Ann. Combust. Liq. **23**, 1349 (1968).
[52] L. Paterson, J. Fluid Mech. **113**, 513 (1981).
[53] J. Nittmann, G. Daccord, and H. E. Stanley, Nature (London) **314**, 141 (1985); in *Fractals in Physics*, edited by L. Pietronero and E. Tosatti (North Holland, Amsterdam, 1986); G. Daccord, J. Nittmann, and H. E. Stanley, Phys. Rev. Lett. **56**, 336 (1986).
[54] J. V. Maher, Phys. Rev. Lett. **54**, 1498 (1985); S. N. Rauseo, P. D. Barnes, and J. V. Maher, Phys. Rev. A **35**, 1245 (1987); S. E. May and J. V. Maher, *ibid.* **40**, 1723 (1989).
[55] J.-D. Chen, J. Fluid Mech. **201**, 223 (1989).
[56] T. Maxworthy, Phys. Rev. A **39**, 5863 (1989).
[57] S. K. Sarkar, Phys. Rev. Lett. **65**, 2680 (1990).
[58] S. B. K. Burns and S. G. Advani, Exp. Fluids **21**, 187 (1996).
[59] M. T. Batchelor and B. I. Henry, Fractals **4**, 149 (1996).
[60] L. Carrillo, F. X. Magdaleno, J. Casademunt, and J. Ortín, Phys. Rev. E **54**, 6260 (1996); L. Carrillo, J. Soriano, and J. Ortín, Phys. Fluids **11**, 778 (1999); **12**, 1685 (2000).
[61] L. Boltzmann, Wien. Ber. **66**, 275 (1872); [English translation in *Kinetic Theory II*, edited by S.G. Brush (Pergamon, Oxford, 1966)].
[62] T. A. Witten and L. M. Sander, Phys. Rev. Lett. **47**, 1400 (1981); Phys. Rev. B **27**, 5686 (1983).
[63] For a review of DLA algorithms, see P. Meakin, in *Phase Transitions and Critical Phenomena*, edited by C. Domb and J. L. Lebowitz (Academic, New York, 1988), Vol. 12, p. 336; L. M. Sander, Contemp. Phys. **41**, 203 (2000), and references therein.
[64] J.-D. Chen and D. Wilkinson, Phys. Rev. Lett. **55**, 1892 (1985).
[65] M. Sahimi and Y. C. Yortsos, Phys. Rev. A **32**, 3762 (1985); M. Sahimi, Rev. Mod. Phys. **65**, 1393 (1993).
[66] D. Y. C. Chan, B. D. Hughes, and L. Paterson, Phys. Rev. A **34**, 4079 (1986); Nature (London) **325**, 489 (1987); D. Y. C. Chan, B. D. Hughes, L. Paterson, and C. Sirakoff, Phys. Rev. A **38**, 4106 (1988).
[67] K. J. Måløy, J. Feder, and T. Jøssang, Phys. Rev. Lett. **55**, 2688 (1985); K. J. Måløy, F. Boger, J. Feder, T. Jøssang, and P. Meakin, Phys. Rev. A **36**, 318 (1987); E. L. Hinrichsen, K. J. Måløy, J. Feder, and T. Jøssang, J. Phys. A **22**, L271 (1989); V. Frette, K. J. Måløy, F. Boger, J. Feder, T. Jøssang, and P. Meakin, Phys. Rev. A **42**, 3432 (1990).
[68] G. M. Homsy, Annu. Rev. Fluid Mech. **19**, 271 (1987).
[69] P. Meakin, Phys. Rev. A **36**, 2833 (1987); P. Meakin, F. Family, and T. Vicsek, J. Colloid Interface Sci. **117**, 394 (1987); P.

Meakin, M. Murat, A. Aharony, J. Feder, and T. Jøssang, Physica A **155**, 1 (1989).
[70] R. B. Selinger, J. Nittmann, and H. E. Stanley, Phys. Rev. A **40**, 2590 (1989).
[71] U. Oxaal, M. Murat, F. Boger, A. Aharony, J. Feder, and T. Jøssang, Nature (London) **329**, 32 (1987); U. Oxaal, Phys. Rev. A **44**, 5038 (1991); U. Oxaal, F. Boger, J. Feder, T. Jøssang, P. Meakin, and A. Aharony, *ibid.* **44**, 6564 (1991).
[72] J. F. Fernández, R. Rangel, and J. Rivero, Phys. Rev. Lett. **67**, 2958 (1991).
[73] M. Ferer, R. A. Geisbrecht, W. N. Sams, and D. H. Smith, Phys. Rev. A **45**, R6973 (1992); M. Ferer and D. H. Smith, Phys. Rev. E **49**, 4114 (1994); M. Ferer, J. C. Gump, and D. H. Smith, *ibid.* **53**, 2502 (1996).
[74] L. Paterson, Phys. Rev. Lett. **52**, 1621 (1984).
[75] C. Tang, Phys. Rev. A **31**, 1977 (1985).
[76] L. P. Kadanoff, J. Stat. Phys. **39**, 267 (1985).
[77] S. K. Sarkar, Phys. Rev. A **32**, 3114 (1985).
[78] T. Vicsek, Phys. Scr. **T19**, 334 (1987).
[79] P. Ramanlal and L. M. Sander, J. Phys. A **21**, L995 (1988).
[80] Z. Koza, J. Phys. A **24**, 4895 (1991).
[81] M. Marsili and E. Caglioti, Physica A **176**, 463 (1991); M. Marsili, J. Phys. A **25**, 3493 (1992).
[82] M. B. Mineev-Weinstein and R. Mainieri, Phys. Rev. Lett. **72**, 880 (1994).
[83] B. K. Johnson and R. F. Sekerka, Phys. Rev. E **52**, 6404 (1995).
[84] T. C. Halsey, Phys. Today **53**(11), 36 (2000).
[85] A. Arnéodo, Y. Couder, G. Grasseau, V. Hakim, and M. Rabaud, Phys. Rev. Lett. **63**, 984 (1989).
[86] A. Arnéodo, J. Elezgaray, M. Tabard, and F. Tallet, Phys. Rev. E **53**, 6200 (1996).
[87] T. Vicsek, Phys. Rev. Lett. **53**, 2281 (1984); Phys. Rev. A **32**, 3084 (1985).
[88] J. R. Banavar, M. Kohmoto, and J. Roberts, Phys. Rev. A **33**, 2065 (1986).
[89] S. Liang, Phys. Rev. A **33**, 2663 (1986).
[90] R. Tao, M. A. Novotny, and K. Kaski, Phys. Rev. A **38**, 1019 (1988).
[91] J. F. Fernández and J. M. Albarrán, Phys. Rev. Lett. **64**, 2133 (1990); H. La Roche, J. F. Fernández, M. Octavio, A. G. Loeser, and C. J. Lobb, Phys. Rev. A **44**, R6185 (1991).
[92] R. C. Ball, Physica A **140**, 62 (1986).
[93] J. Kertész and T. Vicsek, J. Phys. A **19**, L257 (1986).
[94] J. Nittmann and H. E. Stanley, Nature (London) **321**, 663 (1987); J. Phys. A **20**, L1185 (1987); H. E. Stanley, Physica A **163**, 334 (1990).
[95] T. Aukrust, M. A. Novotny, D. A. Browne, and K. Kaski, Phys. Rev. A **39**, 2587 (1989).
[96] P. Meakin, Phys. Rev. A **36**, 332 (1987); J.-P. Eckmann, P. Meakin, I. Procaccia, and R. Zeitak, *ibid.* **39**, 3185 (1989); Phys. Rev. Lett. **65**, 52 (1990).
[97] M. T. Batchelor and B. I. Henry, Phys. Rev. A **45**, 4180 (1992); Physica A **187**, 551 (1992); **233**, 905 (1996); M. T. Batchelor, C. R. Dun, and B. I. Henry, *ibid.* **193**, 553 (1993).
[98] R.-F. Xiao, J. I. D. Alexander, and F. Rosenberger, Phys. Rev. A **38**, 2447 (1988); **43**, 2977 (1991); J. Cryst. Growth **100**, 313 (1990).
[99] S. Ohta and H. Honjo, Physica A **44**, 8425 (1991).
[100] V. A. Bogoyavlenskiy and N. A. Chernova, Phys. Rev. E **61**, 1629 (2000).
[101] M. Nauenberg, Phys. Rev. B **28**, 449 (1983); M. Nauenberg, R. Richter, and L. M. Sander, *ibid.* **28**, 1649 (1983); M. Nauenberg and L. M. Sander, Physica A **123**, 360 (1984); R. Ball, M. Nauenberg, and T. A. Witten, Phys. Rev. A **29**, 2017 (1984).
[102] P. Garik, R. Richter, J. Hautman, and P. Ramanlal, Phys. Rev. A **32**, 3156 (1985); L. M. Sander, P. Ramanlal, and E. Ben-Jacob, *ibid.* **32**, 3160 (1985).
[103] Y. Kantor, T. A. Witten, and R. C. Ball, Phys. Rev. A **33**, 3341 (1986).
[104] M. E. Cates, Phys. Rev. A **34**, 5007 (1986); K. Kassner, *ibid.* **42**, 3637 (1990).
[105] E. Brener, H. Levine, and Y. Tu, Phys. Rev. Lett. **66**, 1978 (1991); H. Levine and Y. Tu, Phys. Rev. A **45**, 1044 (1992); **45**, 1053 (1992).
[106] S. Sandow and S. Trimper, Europhys. Lett. **21**, 799 (1993).
[107] H. Levine and Y. Tu, Phys. Rev. E **48**, R4207 (1993).
[108] K. Kassner and E. Brener, Phys. Rev. E **50**, 2161 (1994).
[109] P. Keblinski, A. Maritan, F. Toigo, and J. R. Banavar, Phys. Rev. E **49**, R4795 (1994); P. Keblinski, A. Maritan, F. Toigo, R. Messier, and J. R. Banavar, *ibid.* **53**, 759 (1996).
[110] D. A. Kessler, Philos. Mag. B **77**, 1313 (1998).
[111] V. A. Bogoyavlenskiy and N. A. Chernova, Phys. Rev. E **61**, 5422 (2000).
[112] V. A. Bogoyavlenskiy, Phys. Rev. E **63**, 045305(R) (2001).
[113] A. Arnéodo, F. Argoul, E. Bacry, J. F. Muzy, and M. Tabard, Phys. Rev. Lett. **68**, 3456 (1992); A. Arnéodo, F. Argoul, J. F. Muzy, and M. Tabard, Physica A **188**, 217 (1992).
[114] D. A. Kessler, Z. Olami, J. Oz, I. Procaccia, E. Somfai, and L. M. Sander, Phys. Rev. E **57**, 6913 (1998).
[115] R. C. Ball and R. M. Brady, J. Phys. A **18**, L809 (1985); R. C. Ball, R. M. Brady, G. Rossi, and B. R. Thompson, Phys. Rev. Lett. **55**, 1406 (1985).
[116] F. Family, T. Vicsek, and B. Taggett, J. Phys. A **19**, L727 (1986); P. Meakin and T. Vicsek, in *Fractals in Physics*, edited by L. Pietronero and E. Tosatti (North Holland, Amsterdam, 1986), p. 213.
[117] P. Meakin, Phys. Rev. A **33**, 3371 (1986); P. Meakin, R. C. Ball, P. Ramanlal, and L. M. Sander, *ibid.* **35**, 5233 (1987).
[118] Y. Couder, F. Argoul, A. Arnéodo, J. Maurer, and M. Rabaud, Phys. Rev. A **42**, 3499 (1990); A. Arnéodo, F. Argoul, Y. Couder, and M. Rabaud, Phys. Rev. Lett. **66**, 2332 (1991).
[119] Y. Kim, K. R. Choi, and H. Pak, Phys. Rev. A **45**, 5805 (1992); Y. Kim and K. R. Choi, Phys. Rev. E **48**, 1586 (1993); Y. Kim and S. H. Park, *ibid.* **49**, 1763 (1994).
[120] V. A. Bogoyavlenskiy, Phys. Rev. E **63**, 011602 (2001).
[121] E. Ben-Jacob, R. Godbey, N. D. Goldenfeld, J. Koplik, H. Levine, T. Mueller, and L. M. Sander, Phys. Rev. Lett. **55**, 1315 (1985); E. Ben-Jacob, P. Garik, T. Mueller, and D. Grier, Phys. Rev. A **38**, 1370 (1988).
[122] Y. Couder, O. Cardoso, D. Dupuy, P. Tavernier, and W. Thom, Europhys. Lett. **2**, 437 (1986).
[123] Á. Buka, J. Kertész, and T. Vicsek, Nature (London) **323**, 424 (1986); Á. Buka and P. Palffy-Muhoray, Phys. Rev. A **36**, 1527 (1987); Á. Buka, P. Palffy-Muhoray, and Z. Rácz, *ibid.* **36**, 3984 (1987); Á. Buka, Phys. Scr. **T25**, 114 (1989); in *Pattern Formation in Liquid Crystals*, edited by Á. Buka and

L. Kramer (Springer, New York, 1996).
[124] V. Horváth, T. Vicsek, and J. Kertész, Phys. Rev. A **35**, 2353 (1987); V. Horváth, J. Kertész, and T. Vicsek, Europhys. Lett. **4**, 1133 (1987).
[125] J.-D. Chen, Exp. Fluids **5**, 363 (1987).
[126] S. K. Sarkar and D. Jasnow, Phys. Rev. A **39**, 5299 (1989).
[127] L. Lam, H. C. Morris, R. F. Shao, S. L. Yang, Z. C. Liang, S. Zheng, and H. Liu, Liq. Cryst. **5**, 1813 (1989); L. Lam, in *Wave Phenomena*, edited by L. Lam and H. C. Morris (Springer, New York, 1989); S. L. Yang, Z. C. Liang, R. F. Shao, and L. Lam, in *Wave Phenomena*, edited by L. Lam and H. C. Morris (Springer, New York, 1989)].
[128] M. Ben Amar, R. Combescot, and Y. Couder, Phys. Rev. Lett. **70**, 3047 (1993).
[129] K. V. McCloud and J. V. Maher, Phys. Rev. E **51**, 1184 (1995); **54**, 1625 (1996); J. Ignés-Mullol and J. V. Maher, *ibid.* **53**, 3788 (1996).
[130] M. Kawaguchi, A. Shibata, K. Shimomoto, and T. Kato, Phys. Rev. E **58**, 785 (1998); M. Kawaguchi, K. Shimomoto, A. Shibata, and T. Kato, Chaos **9**, 323 (1999); M. Kawaguchi, Macromol. Symp. **160**, 85 (2000).
[131] A. G. Banpurkar, A. V. Limaye, and S. B. Ogale, Phys. Rev. E **61**, 5507 (2000).
[132] R. Folch, J. Casademunt, and A. Hernández-Machado, Phys. Rev. E **61**, 6632 (2000).